VISUAL DESIGN & ACADEMIC STUDIES COORDINATION OFFICE

Nabi SARIBAŞ - Selin YILMAZ - Elif ERMAN

PRINTED BY

CONTENTS

From the Editor

International Journal of Electronics, Mechanical and Mechatronics Engineering (IJEMME), is an international multi-disciplinary journal dedicated to disseminate original, high-quality analytical and experimental research articles on Robotics, Mechanics, Electronics, Telecommunications, Control Systems, System Engineering, Biomedical and Renewable Energy Technologies. Contributions are expected to have relevance to an industry, an industrial process, or a device. Subject areas could be as narrow as a specific phenomenon or a device or as broad as a system.

The manuscripts to be published are selected after a peer review process carried out by our board of experts and scientists. Our aim is to establish a publication which will be abstracted and indexed in the Engineering Index (EI) and Science Citation Index (SCI) in the near future. The journal has a short processing period to encourage young scientists.

Prof. Dr. Hasan HEPERKAN
Editor
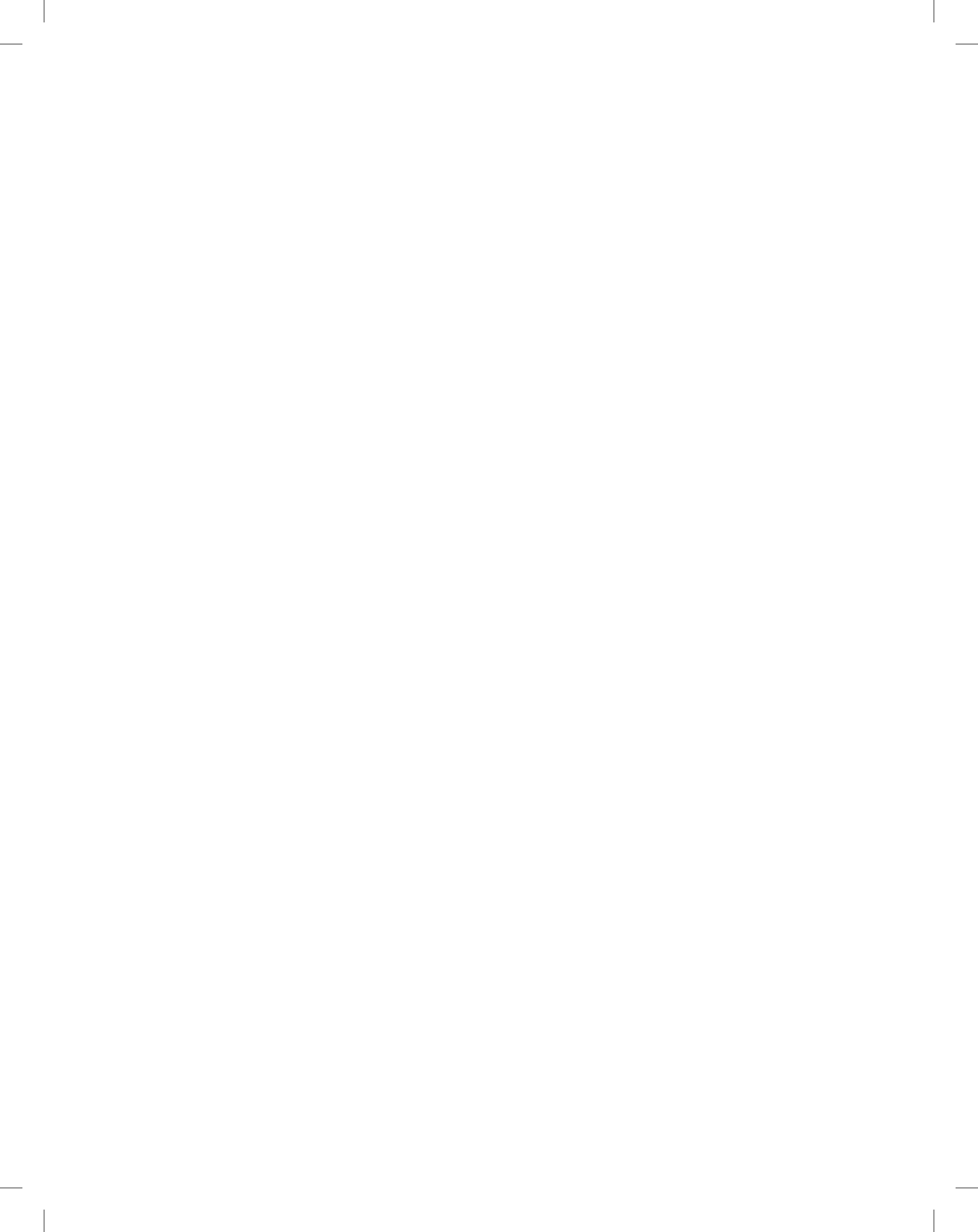
Investigation of Performance Analysis of an Existing Building with Nonlinear Method

Mehmet Fatih ALTAN[1], Uğur DEMİR[2]

Abstract - In recent years, civil engineers have been turning to nonlinear static analysis or thrust analysis, which directly estimates the amount and location of plastic flow in a building, repairing or strengthening of structures built before the situation in Turkey and analysis may be required, durability, stiffness or assumptions regarding ductility may not be reliable. In an existing building, seismic performance evaluation was made using nonlinear analysis and a number of results were obtained by considering the capacity spectrum method and the displacement coefficient method as a performance-based analysis method.

Keywords: *Pushover Analysis, Capacity Spectrum Method, Displacement Coefficient Method, Seismic Performance*

1. Introduction

In general, a building needs to be modeled and analyzed as a three-dimensional combination of its elements and components. It is important that all elements that are part of the lateral or vertical load system and have significant rigidity or limited deformation capacity are represented in the analytical model. The elastic and inelastic strength and stiffness characteristics of each element should be modeled to the extent that their important influence on the response of the building is reasonably represented.

If the elements have inelastic deformation capacity but the strength attenuation does not necessarily lead to unacceptable performance, force deformation models should include the post-distortion interval as shown in figure 1. In a typical building, almost all elements, including many non-structural components, will contribute to the overall rigidity, mass, damping of the building and, consequently, its response to earthquake ground motion.

The general force and deformation curves used to indicate component modeling and acceptance criteria for deformation controlled actions in any of the four basic material types are shown in figure 1. Elements and components that provide the capacity to withstand collapse under seismic forces induced by ground motion in any direction are

---

[1] *Prof., Department of Civil Engineering, Istanbul Aydin University, Istanbul, Turkey, e-mail: mehmetaltan@aydin.edu.tr, https://orcid.org/0000-0003-0961-0115*
[2] *Department of Civil Engineering, Istanbul Aydin University, Istanbul, Turkey.*

classified as primary. Other elements and components are classified as secondary. A linear response is depicted between point A (no-load component) and an effective pour point B. The slope from B to C is typically a small percentage (0-10%) of the elastic slope and is included to represent phenomena such as strain stiffening. C has a coordinate representing the strength of the element and an apse value equal to the deformation at which significant strength degradation begins. Beyond point D, the element responds to point E with significantly reduced strength. For deformations larger than point E, the element strength is essentially zero.
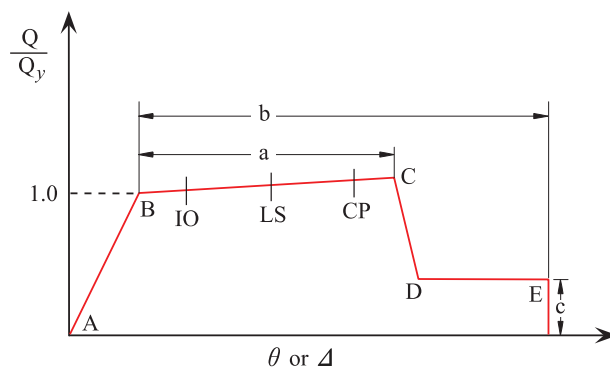
Figure 1: Element Deformation [1]

As shown in the idealized curves between points C and D in Figure 1, sharp transition may result in computational difficulty and convergence failure when used as a modeling input in nonlinear computerized analysis software. To avoid this computational imbalance, a small slope can be provided to the segment of these curves between points C and D.

- CP: Creating Crash Prevention Performance Levels
- LS: Life safety
- IO: Immediate occupancy

As shown in Figure 1, five points labeled A, B, C, D and E are used to define the load deviation behavior of the joint, and three points labeled CP, LS and IO are used to define the acceptance criteria for the joint. Modeling is one of the important steps in the implementation of push analysis. The model should take into account the nonlinear behavior of the structural members, which requires determining the component measured by the strength and deformation capacities in the structure. The final deformation capacity of a component depends on the final curvature and plastic hinge length. Using different criteria for the final curvature and different plastic hinge length may result in different deformation capacities [2].

2. Materials and Methods

In general, nonlinear analysis methods provide more useful and more accurate results than linear methods. If a load irregularity exists and concentrates on a single layer, the nonlinear static method is expected to provide good estimates about the displacement and load demand parameters. an invariant load model is unlikely to detect more than one

irregularity. In such cases, nonlinear response history analysis is recommended. The application of nonlinear single mode push analysis is discussed below.

Number of Story :	7
Building Height :	21.42 (m)
Building Height Above Rigid Basement :	18.00 (m)
Rigid of Basement Story Number :	1
Rigid Basement Story :	-1
Maximum Story Height :	3.50 (m)
Maximum Beam Clearance :	7.04 (m)
Planned Usage :	Home + Shop
Number of Rigid Diaphragms :	7

Columns :	C30 S420
Shear Walls :	C30 S420
Beams :	C30 S420
Slabs :	C30 S420
Foundations :	C30 S420
Concrete Safety Coefficient :	1.50
Reinforcement Safety Coefficient :	1.15
Concrete Unit Volume Weight :	2.50

(a)   (b)

Figure 2: (a) Structure geometric information (b) Material information

Building Importance Factor (I) :	1
Building Usage Class (BUC) :	3
Carrier System Behavior Coefficient (Entered) (X/Y) :	1
Carrier System Behavior Coefficient (Selected) (X/Y) :	1
Strength Excess Coefficient (X/Y) :	1
Eccentricity Ratio :	0.05
Ductility Level :	High
Earthquake Ground Motion Level :	DD-2
Earthquake Design Class (EDC) :	1
Building Height Class (BHC) :	5
Normal Performance Destination :	Controlled Damage
Evaluation / Design Approach :	Assessment and Design by Strain
Soil Type :	ZC
Spectrum Characteristic Periods :	Ta : 0.07, Tb : 0.33
Bearing Capacity of Soil:	
Coefficient of Soil Reaction :	
Short Period Map Spectral Acceleration Coefficient (Ss) :	1.198
Map Spectral Acceleration Coefficient for 1.0 Second Period (S1) :	0.312
Short Period Design Spectral Acceleration Coefficient (SDs) :	1.438
Design Spectral Acceleration Coefficient for a 1.0 Second Period (SD1) :	0.468
The Biggest Place Acceleration (g) (PGA) :	0.492
Maximum Place Speed (PGV) :	31.314

Figure 3: Earthquake parameters and soil parameters

Table 1: Loads in the Structure

Load States	Explanation
G	Dead Load
Q	Live Load
EX	Static Earthquake Load
EY	Static Earthquake Load
SPX	Horizontal Elastic Design Spectrum
SPY	Horizontal Elastic Design Spectrum
PUSH0	Nonlinear Vertical Load
PUSHX	Nonlinear Pushover Load
PUSHY	Nonlinear Pushover Load

G	Dead Load
Q	Live Load
EX	Static Earthquake Load

Table 2: Load combinations

Load Combinations
1.4G+1.6Q
G+0.3Q G+Q+EX
G+Q+SPX G+Q+EY
G+Q+SPY 0.9G+EX
0.9G+SPX 0.9G+EY
0.9G+SPY G+0.3Q+EX+0.3EY
G+0.3Q+SPX+0.3SPY G+0.3Q+EX-0.3EY
G+0.3Q+SPX-0.3SPY G+0.3Q-EX-03EY
G+0.3Q-SPX-0.3SPY G+0.3Q-EX+0.3EY
G+0.3Q-SPX+0.3SPY G+0.3Q+EY+0.3EX
G+0.3Q+SPY+0.3SPX G+0.3Q-EY-0.3EX
G+0.3Q-SPY-0.3SPX
1.4G+1.6Q
G+0.3Q G+Q+EX
G+Q+SPX G+Q+EY
G+Q+SPY 0.9G+EX
0.9G+SPX 0.9G+EY
0.9G+SPY G+0.3Q+EX+0.3EY
G+0.3Q+SPX+0.3SPY G+0.3Q+EX-0.3EY
G+0.3Q+SPX-0.3SPY G+0.3Q-EX-03EY
G+0.3Q-SPX-0.3SPY G+0.3Q-EX+0.3EY
G+0.3Q-SPX+0.3SPY G+0.3Q+EY+0.3EX
G+0.3Q+SPY+0.3SPX G+0.3Q-EY-0.3EX
G+0.3Q-SPY-0.3SPX

In this study, TS 500 (February 2000), TBDY 2018, ATC-40 standards and regulations were used.

2.1. Linear Analysis

Structure displacement for modal account coverage is expressed as a combination of displacement in each mode. In each mode, the structure is analyzed as a single-graded system, the resulting force and displacement are combined in proportion to the participation (weight) of the modes. Modal analysis results are given below.
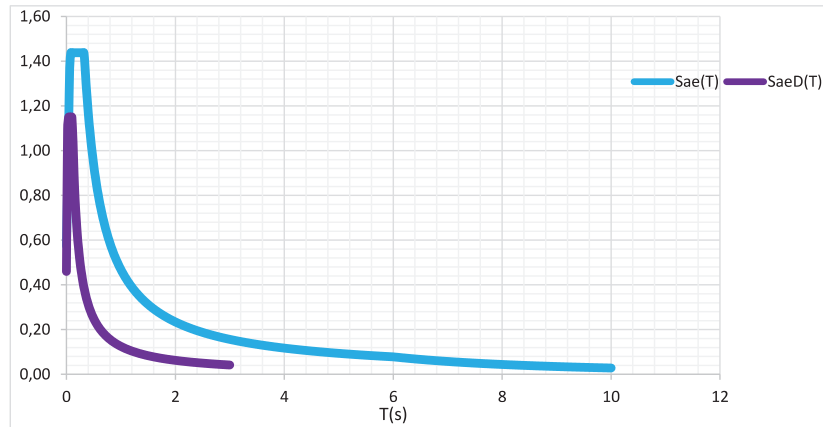
Figure 4: Horizontal spectrum for dynamic loads in the structure

OutputCase	StepType	StepNum	Period	UX	UY	SumUX	SumUY
Text	Text	Unitless	Sec	Unitless	Unitless	Unitless	Unitless
MODAL	Mode	1	1,100	0,0560	0,0783	0,056	0,078
MODAL Y	**Mode**	**2**	**0,904**	**0,1041**	**0,4623**	**0,160**	**0,541**
MODAL X	**Mode**	**3**	**0,815**	**0,5074**	**0,1541**	**0,668**	**0,695**
MODAL	Mode	4	0,330	0,0060	0,0093	0,674	0,704
MODAL	Mode	5	0,251	0,0119	0,0853	0,685	0,789
MODAL	Mode	6	0,199	0,1176	0,0201	0,803	0,809
MODAL	Mode	7	0,168	0,0032	0,0021	0,806	0,811
MODAL	Mode	8	0,141	0,0000	0,0000	0,806	0,811
MODAL	Mode	9	0,139	0,0000	0,0000	0,806	0,811
MODAL	Mode	10	0,138	0,0000	0,0000	0,806	0,811
MODAL	Mode	11	0,137	0,0000	0,0000	0,806	0,811
MODAL	Mode	12	0,136	0,0000	0,0000	0,806	0,811
MODAL	Mode	13	0,136	0,0000	0,0000	0,806	0,811
MODAL	Mode	14	0,135	0,0000	0,0000	0,806	0,811
MODAL	Mode	15	0,135	0,0000	0,0000	0,806	0,811
MODAL	Mode	16	0,134	0,0000	0,0000	0,806	0,811
MODAL	Mode	17	0,134	0,0000	0,0001	0,806	0,811
MODAL	Mode	18	0,134	0,0000	0,0000	0,806	0,811
MODAL	Mode	19	0,133	0,0000	0,0000	0,806	0,811
MODAL	Mode	20	0,121	0,0000	0,0000	0,806	0,811
MODAL	Mode	21	0,120	0,0000	0,0003	0,806	0,812

Figure 5: Modal participating mass ratios

Here, period in X direction: 0.815 s and period in Y direction: 0.904 s.

OutputCase	StepType	StepNum	Period	UX	UY	ModalMass	ModalStiff
Text	Text	Unitless	Sec	KN-m	KN-m	KN-m-s2	KN-m
MODAL	Mode	1	1,100	-0,00037	-0,00044	0,00001	0,00033
MODAL	Mode	2	0,904	0,00051	0,00107	0,00001	0,00048
MODAL	Mode	3	0,815	0,00112	-0,00062	0,00001	0,00059
MODAL	Mode	4	0,330	0,00012	0,00015	0,00001	0,00363
MODAL	Mode	5	0,251	0,00017	0,00046	0,00001	0,00628
MODAL	Mode	6	0,199	-0,00054	0,00022	0,00001	0,01001
MODAL	Mode	7	0,168	-0,00009	-0,00007	0,00001	0,01404
MODAL	Mode	8	0,141	-0,00001	0,00001	0,00001	0,01988
MODAL	Mode	9	0,139	0,00001	0,00000	0,00001	0,02043
MODAL	Mode	10	0,138	-0,00001	0,00000	0,00001	0,02078
MODAL	Mode	11	0,137	0,00000	0,00000	0,00001	0,02108
MODAL	Mode	12	0,136	0,00000	0,00000	0,00001	0,02125
MODAL	Mode	13	0,136	0,00000	0,00000	0,00001	0,02145
MODAL	Mode	14	0,135	0,00000	0,00000	0,00001	0,02154
MODAL	Mode	15	0,135	0,00000	0,00000	0,00001	0,02181
MODAL	Mode	16	0,134	0,00000	0,00000	0,00001	0,02183
MODAL	Mode	17	0,134	0,00000	-0,00001	0,00001	0,02194
MODAL	Mode	18	0,134	0,00000	0,00000	0,00001	0,02211
MODAL	Mode	19	0,133	0,00000	0,00000	0,00001	0,02219
MODAL	Mode	20	0,121	0,00000	0,00001	0,00001	0,02703
MODAL	Mode	21	0,120	-0,00001	-0,00003	0,00001	0,02735

Figure 6: Modal participation factors
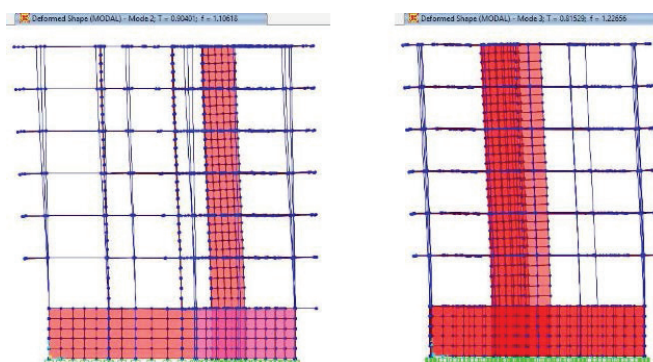
Figure 7: Deformed shapes (Modal)

OutputCase	StepType	StepNum	Period	Frequency	CircFreq	Eigenvalue
Text	Text	Unitless	Sec	Cyc/sec	rad/sec	rad2/sec2
MODAL	Mode	1	1,100	0,909	5,712	32,626
MODAL	Mode	2	0,904	1,106	6,950	48,307
MODAL	Mode	3	0,815	1,227	7,707	59,393
MODAL	Mode	4	0,330	3,030	19,040	362,533
MODAL	Mode	5	0,251	3,988	25,057	627,857
MODAL	Mode	6	0,199	5,035	31,637	1000,881
MODAL	Mode	7	0,168	5,963	37,464	1403,531
MODAL	Mode	8	0,141	7,096	44,587	1987,995
MODAL	Mode	9	0,139	7,194	45,204	2043,392
MODAL	Mode	10	0,138	7,256	45,588	2078,302
MODAL	Mode	11	0,137	7,307	45,908	2107,590
MODAL	Mode	12	0,136	7,336	46,094	2124,660
MODAL	Mode	13	0,136	7,372	46,318	2145,333
MODAL	Mode	14	0,135	7,387	46,414	2154,252
MODAL	Mode	15	0,135	7,432	46,696	2180,510
MODAL	Mode	16	0,134	7,436	46,723	2182,997
MODAL	Mode	17	0,134	7,454	46,836	2193,613
MODAL	Mode	18	0,134	7,484	47,022	2211,049
MODAL	Mode	19	0,133	7,498	47,109	2219,290
MODAL	Mode	20	0,121	8,275	51,994	2703,404
MODAL	Mode	21	0,120	8,323	52,293	2734,556

Figure 8: Modal periods and frequencies

2.2. Nonlinear Single Mode Pushover Analysis

A pushover analysis for determining the behavioral characteristics and performances of the structures under the effect of horizontal loads, is a numerical investigation where the stiffness and strength change are calculated by taking into account the inelastic behavioral characteristics of the building elements in general, and these calculations are defined for certain performance values. Approximate results are produced as the basis of the method is the acceptance of multi degree of freedom systems equivalent to a single degree of freedom system. The analysis method has a suitable procedure for rigid or articulated inelastic frame analysis. This procedure can be considered a different extension of the elastic frame analysis procedure, which is essentially formed with semi-rigid bonds.

Two different calculation methods applied in Pushover analysis; It is displacement-controlled analysis and load-controlled analysis. In the displacement-controlled method, horizontal loading is made until the point where the center of gravity on the top floor (top) of the structure reaches a certain displacement level. In the force-controlled method, the structure is loaded until it reaches a certain horizontal load level. By increasing these loads at certain intervals, the force-displacement relations that occur in the building elements are examined in each step and the level of damage of the structure is determined [3,4,5]. The Pushover analysis shows the change of real (functional) rigidity for loads that reveal inelastic behavior in a frame. Depending on the concept of stiffness factor previously described for the analysis of semi-rigid joints, the use of the plasticity factor to determine changes in the stiffness of the frame members under increased loads will be examined.
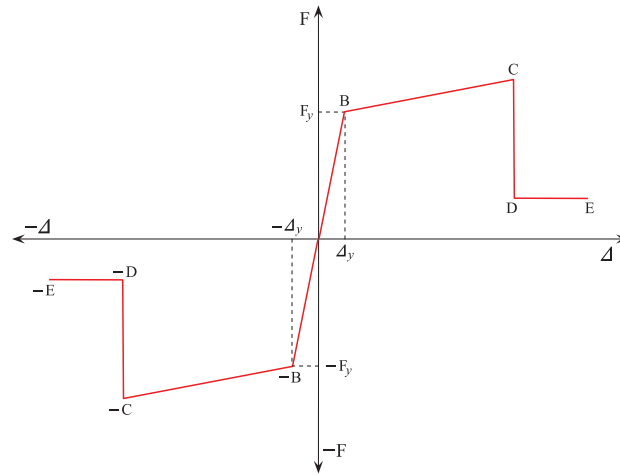
Figure 9: Curve of the F - Δ relationship

Although various methods for nonlinear analysis are determined by regulations, this analysis method, which is still being developed, creates the difficulty of determining the change in the effects against the changing structure stiffness and behavior, and the determination of the rotations in the plastic joints by the procedure for considering various modes of the structure in nonlinear analysis [6, 7, 8]. Thus, different methods are developed and discussed. The procedure given in the FEMA and ATC documents has recently received serious criticism, especially regarding the detection of element joints. In the Pushover analysis, it should be taken into consideration that the error rates are high when examining according to these regulations [9, 10].

Since the values to be determined for floor displacement and floor displacements give more convergent results, it is beneficial to consider these values as a priority in determining the performance of the building [11]. In the general logic of Pushover analysis, there is no cumulative evaluation process in the distribution of flow behavior or plastic hinge formation. It should be remembered that both calculation bases have high error rates in terms of detecting plastic hinge rotations and that results produced especially for irregular structures should therefore be well examined. However, both methods produce good results in regular structures and structural ductility and floor shifts - base shear forces.

(a)   (b)
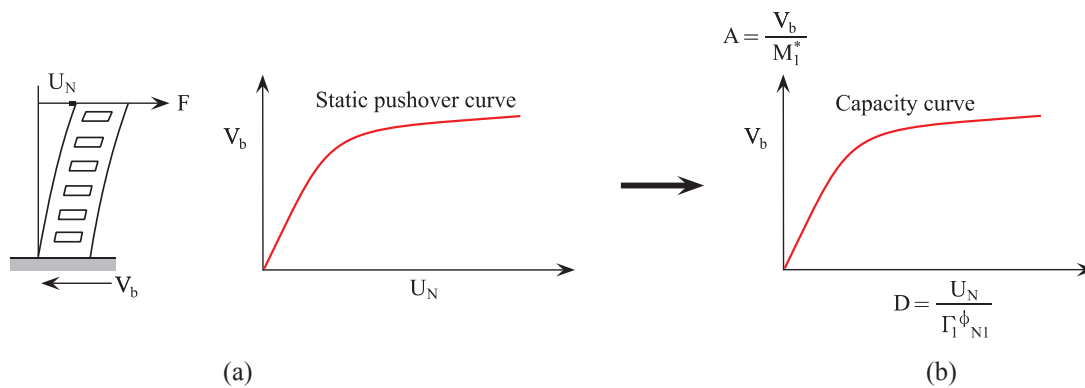
Figure 10: (a) Formation of the pushover curve (b) Converting the pushover curve into a capacity curve

(a)   (b)
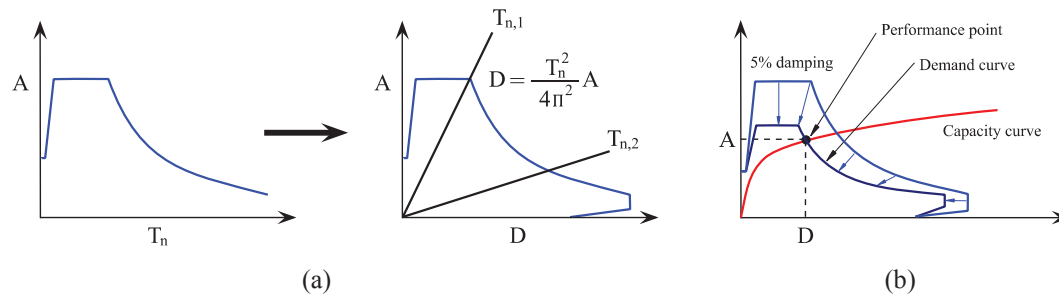
Figure 11: (a) Conversion of the elastic response spectrum from standard format to A-D format (b) Determination of displacement requirement

2.2.1. Determining the Capacity Curve

Creation of two or three dimensional model of the building, determination of the main and secondary carrier elements, ground structure interaction model, defining the second order effects, determining the characteristics of the carrier system elements, defining the cyclical behavior of force-deformation relations, the definition of articulation characters, determining the mutual interaction behavior in columns. [12, 13]. For horizontal load regulation, firstly, determining the vertical loads in the system with appropriate load coefficients, defining horizontal load patterns in both directions positively and negatively, evaluating the effects of torsion and irregularities (here the uniform displacement value for the same displacement value It should be taken into consideration that it will give great base cutting forces).
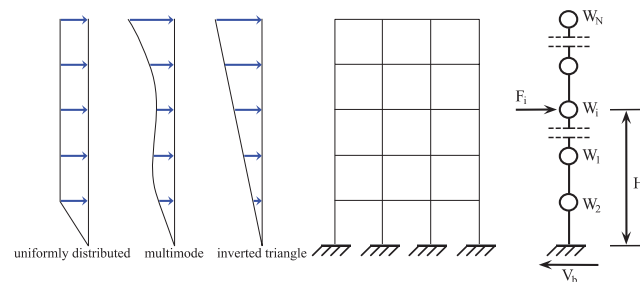
Figure 12: Horizontal load regulation [14]

2.2.2. Determination of Analysis Control Method and Calculations

If we examine this building with the capacity spectrum method ($S_d = S_a T^2/4r^2$); α mass participation (depending on the shear force), the participation factor for the roof displacement of the PF_1 single degree of freedom system is S_a spectral acceleration and S_d spektral displacement.
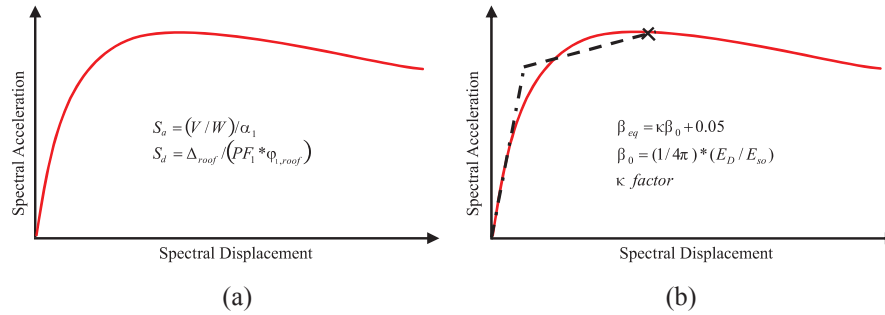
Figure 13: (a) Constructing capacity spectrum (b) Estimation of equivalent viscous damping

3. Results and Discussion

Analysis results were obtained using the finite element method using the SAP2000 program.
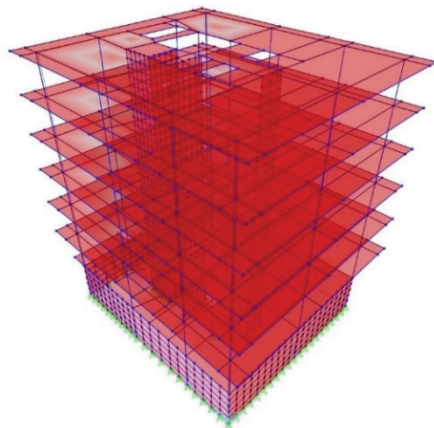
Push Steps (X)		Push Steps (Y)	
Hinge 391		Hinge 391	
Step	Displacement (m)	Step	Displacement (m)
0	-4.98E-01	0	0.00117
1	-0.00167	1	-0.00274
2	-0.01458	2	-0.05484
3	-0.01459	3	-0.1121
4	-0.0217	4	-0.14272
5	-0.0217		
6	-0.05016		
7	-0.05016		
8	-0.10053		
9	-0.1512		
10	-0.15767		

(a) (b)

Figure 14: (a) 3D view of the building (b) Push displacement joint

According to TBDY2018 for the design shear forces taken as the basis for column and beams, if the shear force ratio of 15.7.1.4 - reinforced concrete section with deformation calculation and $V_e / (b_w d f_{ctm}) < 0.65$, the deformation upper limits calculated according to 15.7.1.3 are valid. If the shear force ratio is greater than 1.30, deformation upper limits calculated according to 15.7.1.3 will be reduced by multiplying by 0.50.

Linear interpolation will be applied for intermediate values and V_e will be calculated from equation (1) for beams and equation (2) for columns. In single mode push analysis, let us take the number of pushover steps 10 and G + nQ (KN) as 24300. The modal analysis method we will use is the number 3 in Figure 15 below.

$$V_e = 1.25 f_{yk} \left(A_{s1} + A_{s2} \right) - V_{kol} \tag{1}$$

$$V_e = \frac{M_{\ddot{u}} + M_a}{l_n} \tag{2}$$

Strain borders were determined in columns and beams and analyzed by making comparisons.
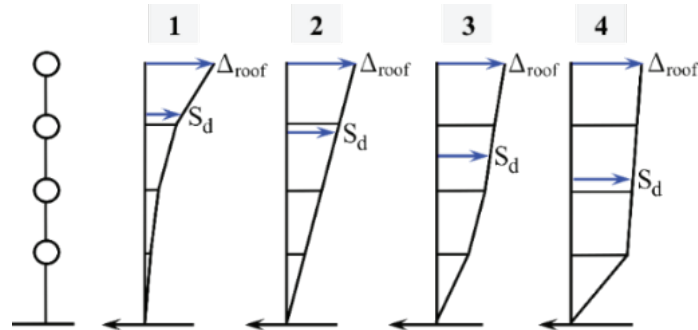
Figure 15: Modal analysis forms [15]

OutputCase	StepType	GlobalFX	GlobalFY	GlobalFZ	GlobalMX	GlobalMY	GlobalMZ
Text	Text	KN	KN	KN	KN-m	KN-m	KN-m
G+0.3Q+SPX+0.3SPY	Max	10171,54	6490,51	24427,90	300962,93	-21515,54	124588,05
G+0.3Q+SPX+0.3SPY	Min	-10171,54	-6490,51	24170,17	106814,31	-325073,24	-124588,06
G+0.3Q+SPX-0.3SPY	Max	10171,54	6490,51	24427,90	300962,93	-21515,54	124588,05
G+0.3Q+SPX-0.3SPY	Min	-10171,54	-6490,51	24170,17	106814,31	-325073,24	-124588,06
G+0.3Q-SPX-0.3SPY	Max	10171,54	6490,51	24427,90	300962,93	-21515,54	124588,05
G+0.3Q-SPX-0.3SPY	Min	-10171,54	-6490,51	24170,17	106814,31	-325073,24	-124588,06
G+0.3Q-SPX+0.3SPY	Max	10171,54	6490,51	24427,90	300962,93	-21515,54	124588,05
G+0.3Q-SPX+0.3SPY	Min	-10171,54	-6490,51	24170,17	106814,31	-325073,24	-124588,06
G+0.3Q+SPY+0.3SPX	Max	6765,49	9254,93	24419,41	344036,80	-72075,90	90885,66
G+0.3Q+SPY+0.3SPX	Min	-6765,49	-9254,93	24178,66	63740,44	-274512,89	-90885,66
G+0.3Q-SPY-0.3SPX	Max	6765,49	9254,93	24419,41	344036,80	-72075,90	90885,66
G+0.3Q-SPY-0.3SPX	Min	-6765,49	-9254,93	24178,66	63740,44	-274512,89	-90885,66

Figure 16: Base shear force
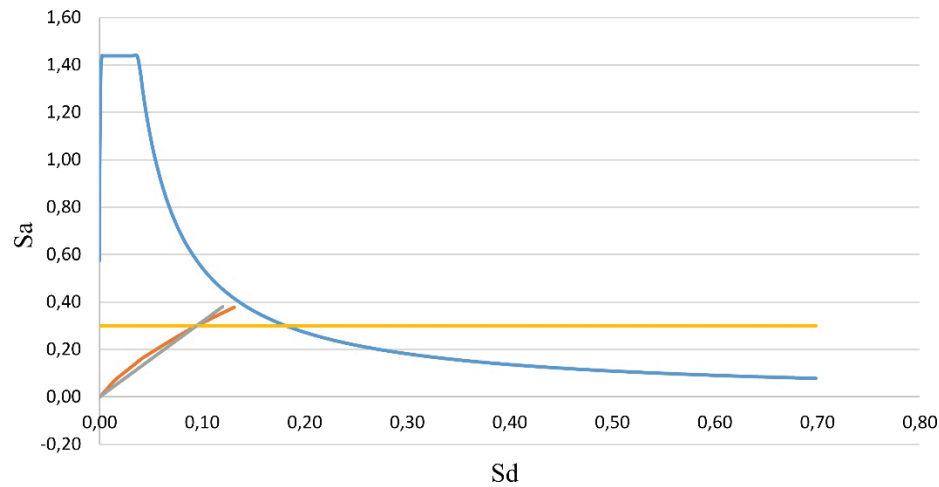
Figure 17: Spectral acceleration and spectral displacement curve

Figure 18: Display plot function traces
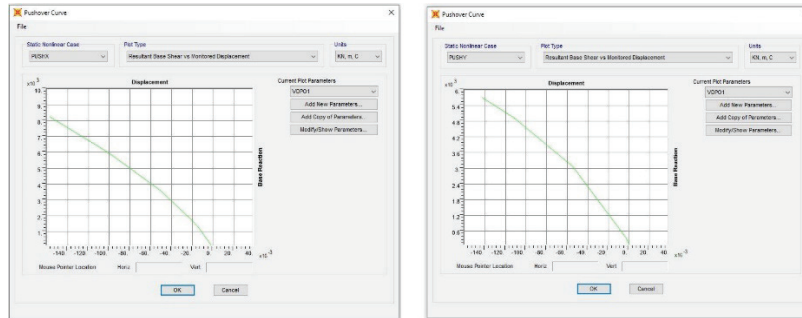
Figure 19: Creating a pushover curve
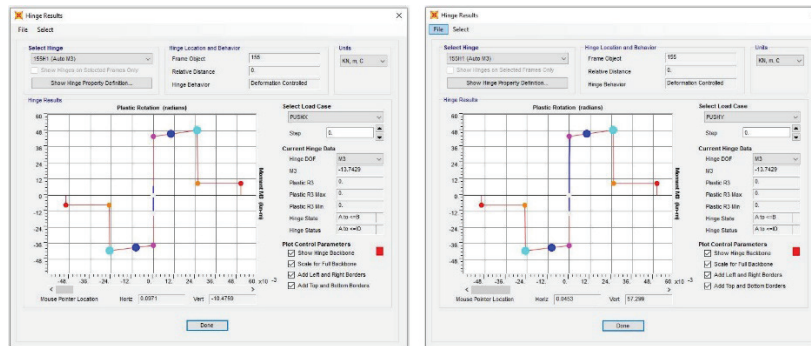
Figure 20: Plastic hinge behavior

LoadCase	Step	Displacement	BaseForce	LoadCase	Step	Displacement	BaseForce
Text	Unitless	m	KN	Text	Unitless	m	KN
PUSHX	0	–0,000498	0	PUSHY	0	0,00117	0
PUSHX	1	–0,001672	115,336	PUSHY	1	–0,002737	325,495
PUSHX	2	–0,014583	1279,592	PUSHY	2	–0,054843	3066,572
PUSHX	3	–0,014588	1278,914	PUSHY	3	–0,112096	4931,475
PUSHX	4	–0,021699	1793,011	PUSHY	4	–0,14272	5708,385
PUSHX	5	–0,021704	1791,54				
PUSHX	6	–0,050156	3567,639				
PUSHX	7	–0,050161	3576,237				
PUSHX	8	–0,100532	5982,031				
PUSHX	9	–0,151201	8003,228				
PUSHX	10	–0,157666	8248,296				

Figure 21: Push capacity diagram

$R_y = 1.9500$ and $C_R = 1$

$d_{1,max} = S_{di}(T_1) = \mathbf{0.16}$ (m) $d_{imax} = $ 0.145 (m) ✓

Base shear force $V_{max} = \mathbf{13000}$ (KN) $V_{max} = $ 10171 (KN) ✓

TA :	0.07
TB :	0.33
TL :	6
T1 :	0.815
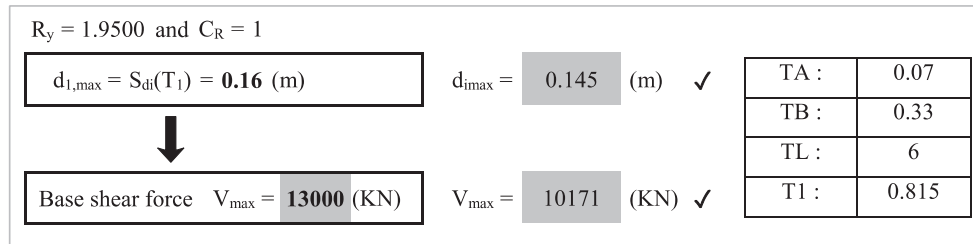
Figure 22: d_{imax} - V_{max}

Adım	D (m)	V (KN)	Sd	Sa
0	0.000498	0	0.000415	0
1	0.001672	115.336	0.001393333	0.005274
2	0.014583	1279.592	0.0121525	0.058509
3	0.014588	1278.914	0.012156667	0.058478
4	0.021699	1793.011	0.0180825	0.081985
5	0.021704	1791.54	0.018086667	0.081918
6	0.050156	3567.639	0.041796667	0.163129
7	0.050161	3576.237	0.041800833	0.163522
8	0.100532	5982.031	0.083776667	0.273527
9	0.151201	8003.228	0.126000833	0.365945
10	0.157666	8248.296	0.131388333	0.377151

Figure 23: Pushover capacity diagram

4. Conclusion and Suggestions

Ordinary response spectrum analysis for elastic high-rise buildings can be reformulated as nonlinear push analysis. The peak response of an elastic structure, which is subjected to lateral loading by push analysis, can be estimated and can provide accurate seismic demand prediction in unsymmetrical structures. Analyzing the behavior of the beam column joints and the failure of plastic joints can be an effective and useful approach. Controlled damage performance level in existing buildings is considered to be at the level of controlled damage performance, provided that the brittle damaged elements are reinforced, provided that:

- Up to 35% of beams and vertical elements (columns,curtains and reinforced partition walls) in any floor of reinforced concrete buildings, excluding secondary beams (not included in the horizontal load bearing system) as a result of the calculation made for each earthquake direction applied as many as defined in the paragraph below can proceed to the advanced damage zone.
- The total contribution of the vertical elements in the advanced damage zone to the shear force carried by the vertical elements on each floor should be below 20%. The ratio of the total shear forces of the vertical elements in the forward damage area to the top floor to the sum of the shear forces of all vertical elements on that floor can be at most 40%.

Table 3: Number of beams crossing the border

Stories	Number of beams	Number of Elements Crossing the Border	%	Control
5 st story	61	4	6	✓
4 st story	64	3	5	✓
3 st story	64	4	6	✓
2 st story	64	3	5	✓
1 st story	64	0	0	✓
Ground Floor	64	0	0	✓
1st Basement Floor	29	0	0	✓

Frame	Station	OutputCase	CaseType	StepType	V2	V2
Text	m	Text	Text	Text	KN	Control
20	0.15	G+0.3Q+SPX+0.3SPY	Combination	Max	126.517	3.98%
21	0.15	G+0.3Q+SPX+0.3SPY	Combination	Max	340.937	10.73%
22	0.15	G+0.3Q+SPX+0.3SPY	Combination	Max	126.22	3.97%
23	0.14999	G+0.3Q+SPX+0.3SPY	Combination	Max	179.79	5.66%
24	0.14999	G+0.3Q+SPX+0.3SPY	Combination	Max	219.933	6.92%
25	0.15	G+0.3Q+SPX+0.3SPY	Combination	Max	190.478	5.99%
26	0.15	G+0.3Q+SPX+0.3SPY	Combination	Max	450.28	14.17%
27	0.15	G+0.3Q+SPX+0.3SPY	Combination	Max	487.014	15.32%
28	0.15	G+0.3Q+SPX+0.3SPY	Combination	Max	437.389	13.76%
29	0.14999	G+0.3Q+SPX+0.3SPY	Combination	Max	203.866	6.41%
30	0.14999	G+0.3Q+SPX+0.3SPY	Combination	Max	163.664	5.15%
31	0.15	G+0.3Q+SPX+0.3SPY	Combination	Max	119.42	3.76%
32	0.15	G+0.3Q+SPX+0.3SPY	Combination	Max	132.88	4.18%
			Total	Max	3178.388	100.00%

Figure 24: Control of ground story columns

Curtain walls with higher rigidity make dynamic analysis easier and simpler. Taking into account the shear effects and applying the unbalanced force approach is essential for a safe and realistic seismic response. If the earthquake loads are large, joints can form in the beams near the middle opening. In such cases, cyclic loads gradually increase the rotation of the joints and cause the beam to sag. Concrete beams are often fragile at shear forces and are therefore designed for flexural strength.
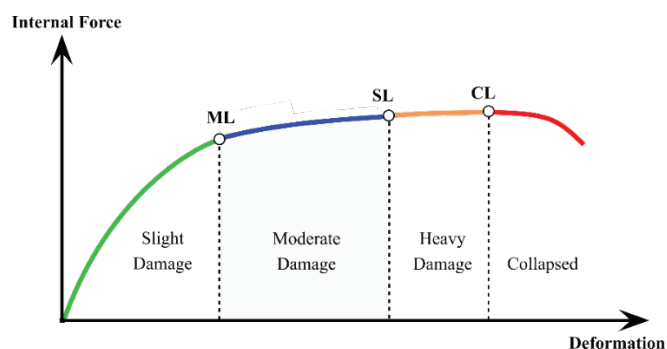
Figure 25: Section damage levels.

Mehmet Fatih ALTAN, Uğur DEMİR

Axial force - moment interactions are additionally required for the columns because the flexural strength depends on the axial force and vice versa. In addition, moments and shear forces move along two axes and force - moment values and interactions affect shear strength. Due to these mutual relationships, the hinge behavior is complex. The building we examined, according to the nonlinear analysis (Single mode push analysis), remained on the border of controlled damage (Distinctive damage zone). However, it is possible to say that the capacity spectrum and the displacement coefficient methods both give close results in the analysis of symmetrical structures. But these methods should be used with caution, as they differ in complex and large structures. Nonlinear time history analysis is essential for such cases.

References

[1] Suharwardy M I. (1999). Static Pushover Analysis for Seismic Design.

[2] Erkan M. (2005). Performans Bazlı Tasarım İtme Analizi - Temel Kavramlar ve Metot.

[3] Hakim R. A., Alama M. S., Ashour S. A. (2014). Seismic Assessment of RC Building According to ATC 40, FEMA 356 and FEMA 440.

[4] Nahavandi H. (2015). Pushover Analysis of Retrofitted Reinforced Concrete Buildings.

[5] FEMA P440A. (2009). Effects of Strength and Stiffness Degradation on Seismic Response.

[6] NEHRP Consultants Joint Venture. (2010). Applicability of Nonlinear Multiple Degree of Freedom Modeling for Design.

[7] Korkmaz K. A., Irtem E. (2008). Evaluation of Previous And Current Performance Based Analysis Methods.

[8] Chopra A. K., Goel R. K. (2002). Capacity-Demand-Diagram Methods For Estimating Deformation of Inelastic Systems.

[9] Leslie R. (2010). The Pushover Analysis, Explained in Its Simplicity.

[10] Demir A., Başaran H., Bağci M. (2014). A Comparative Assessment of Existing Structure By Performance Based Analyses.

[11] Manjula N.K., Nagarajan P., Madhavan Pillai T. M. M. (2013). A Comparison of Basic Pushover Methods.

[12] Prasad B. K. R., Ramaiah A. S. and Singh A. K. (2004). Capacity Spectrum For Structures Asymmetric In Plan.

[13] Dey A., Bhattacharjee U., Sagar V., Utkarsh and Saha P. (2015). Pushover Analysis for Multistory Building.

[14] Lin Y. Y., Chang K. C. and Wang Y. L. (2004). Comparison of Displacement Coefficient Method And Capacity Spectrum Method With Experimental Results Of RC Columns.

[15] TBDY-2018

Ground-Penetration Radar Signal Processing For Water Detection

Sarah Ayad TABANNA[1], İlknur HOŞ[2], Mohanad Abd SHEHAB[3], Saeid KARAMZADEH[4]

ABSTRACT

Ground penetration radar is very promising technology for underground or behind walls detection with high resolution. Recently various development has been introduced in GPR signal processing, multispectral sensors have been used over the years to collect the underground images. In the term of detecting and identify water underground GPR will detect water either by the voids created in the soil or by detecting the anomalies in the depth as the velocity of propagation changes due to the soil saturation with the water. The potential of ground penetration radar for water detection is affected by the type of soils, soil conductivity is an important factor, conductive soils like clay and moist tend to distort the signals which makes it hard to obtain good information about the underground structures.

In this study the aim was to detect underground water and removing clutter and noises represented by different soil situations, multiple signal processing methods has been implemented such as PCA, ICA, PICA and few filtering methods such as Gaussian, Median and compared their capabilities to find the best method in different soil situations.

I. INTRODUCTION

As known GPR technology has been widely used as a method of non-destructive testing of different subsurface observation. The vertical cross-section images obtained allow the identification of thickness and lithological horizons of different media. And over these years, GPR has been able to adjust to new areas [1]. Figure 1 shows the GPR principle. Recently, it has been successfully used to characterize and map subaqueous and anthropogenic soils. It has also been extensively used in hydro-pedological and hydro-geophysical investigations, finding landmines, water, oil, pipes and fused wires. During all GPR surveys, noise in general (either environmental or systematic) with other radio frequency signals interference can blur and damage the desired signal. Meanwhile, clutter which can be something such as a strong reflection from the antenna direct coupling and air-ground subsurface, the signature signals of the subsurface be masked [3- 9].

[1] Electrical and Electronics Engineering, Engineering Faculty, Istanbul Aydin University, Istanbul, Turkey.
[2] Application & Research Center for Advanced Studies, Istanbul Aydin University, Istanbul, Turkey.
[3] Engineering Department, Engineering College, Mustansiriyah University, Baghdad, Iraq.
[4] Electrical and Electronics Engineering Department, Faculty of Engineering and Natural Sciences, Bahçeşehir University, Istanbul, Turkey, https://orcid.org/0000-0003-0669-0746
Corresponding author: Saeid Karamzadeh (karamzadeh@itu.edu.tr).

A considerable number of researches in literature on GPR signal processing multiple signal enhancement and clutter removal methods for underground water detection has been under studying for many years a lot of fresh water is wasted (leaked) throughout the years. Moreover, a recorded response of the radar at a certain location is called an A-Scan waveform, which is explained as a measure of the amplitude in a reflected signal with respect to time. After combining all the collected A-scans by moving the radar antenna in a distinct direction the combined data forms what is called B-scan. In a B-scan image, EM wave transmission time (or penetration depth) is represented by the vertical axis and the horizontal axis represents the GPR spatial location [2].
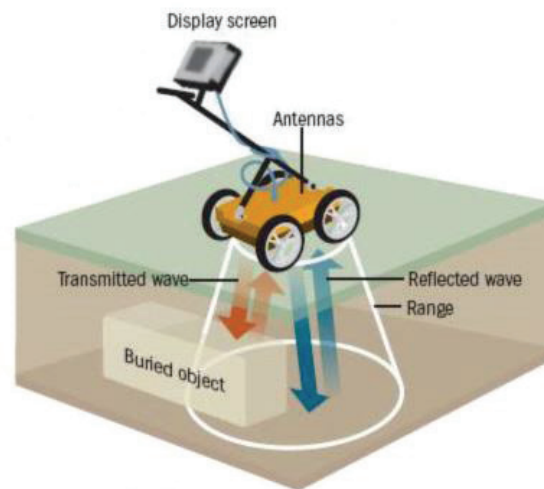
Figure 1: shows basic principle of GPR.

The efficiency of GPR is affected strongly by the soil's conductivity and its dielectric permittivity, since soils have different electrical characteristics so the scan depth is highly dependent on the specific target site. Clay soils, along with brackish or salty water will cause the radar signal to be absorbed or greatly attenuated. So, in certain soil types the GPR depth is limited [4]. So as known in GPR system, the reflected signal is a combination of the target, clutter and system noises. There are different approaches to remove or reduce cluttering in GPR images, the subspace methods such as principle component analysis (PCA) [10], independent component analysis (ICA) [11], singular value decomposition (SVD) [12], and the Probabilistic independent analysis (PICA) or noisy ICA [13]. Many researches were proved that the use of these methods is the best in obtaining the ideal target and they can successfully remove cluttering part from GPR images. GPR signals are almost of non-Gaussian distribution and above the second order moments, as a result ICA is effective to process these types of signals. Moreover, the PCA is simple and adequate for dimensionality reduction, therefore, combining PCA and ICA, i.e., PICA can produce an efficient method that handles both dimensionality reduction with suitable GPR clutter removal.

In this work a box filled with soil and fresh water was implemented inside, data was collected using GPRMax simulation the antenna scanned every 5mm, then roughness was added to the box, new data has been collected with the antenna scanning every 5mm. The last situation 300 blades of grass were implemented on top of this box again new data set was collected. The results of all these methods will be compared and showed to find the best method for these different soil situations.

II.   THE PROPOSED STATISTICAL CLUTTER REDUCTION TECHNIQUES

In GPR systems, the transmitting and receiving antennas are moved in a linear way along the subsurface to transmit waves and detect the reflecting waves from the soil. This displacement produces a set of time or frequency signals named traces at each spatial step; N is the number of spatial   samples and M is the number of time or frequency samples. Therefor the collected data can be expressed in a data matrix X ($M \times N$), where N<M; with a data sample X_{ij}, i is the frequency (time) index and j is the GPR position index.

Different methods have been employed to find such a linear representation, including conventional methods, singular value decomposition, principal components analysis, independent component analysis, etc. along with some filtering techniques such as Gaussian, Median, Wiener and Histogram are used in this research. The simplest conventional clutter removal algorithm is the mean subtraction (MS) which can be expressed as [14][15]:

$$X_{ij} = A_{ij} - \frac{1}{n}\sum_{j=1}^{n} A_{ij} \tag{1}$$

While A is also an $M \times N$ transformation matrix that has Eigen vectors in their decreasing order. After finding the matrix A, the subspace matrixes S_i, A_i and X can be formulated according to the subspace methods

PCA

$$X = \sum_{i=0}^{n} A_i^T S_i \tag{2}$$

ICA

$$X = \sum_{i=0}^{n} A_i S_i \tag{3}$$

SVD

$$X = UDV^T \tag{4}$$

Where $U_{m \times m}, V_{n \times n}$ are orthogonal matrices, $D_{m \times n}$ is a diagonal matrix with singular values arranged in descending order.

$$X = \sum_{i-0}^{n} D_i U_i V_i^T \tag{5}$$

III.   IMAGE PROCESSING FILTERS

In image processing the term filtering is known as technique used for adjustment or image enhancement. As a simple example, you can use a filter on an image to focus on some specific features or disregard other features. So many image processing operations is performed with filtering which includes smoothen, edge enhancement, and sharpening of an image [16][17].

GAUSSIAN FILTER

The Gaussian filters are linear filters with the chosen weights according to the gaussian function shape. So, the Gaussian smoothing filter is a quite good filter for removing noises drawn from normal distribution.

MEDIAN FILTER

The median filter (MF) is non-linear digital filtering technique that can be used to remove noises from images or signals. like a noise reduction method is a classical stage in preprocessing to amend the results of the processing such

as, edge detection on an image. To be very specific, the MF replaces the pixel by the median instead of the average of all pixels in the neighborhood W:

$$y[m,n] = median\{x[i,j], (i,j) \in W \qquad (6)$$

Where W is representing the neighborhood, which is defined by the user, centered in the image around the location [m, n].

WINERE FILTER

The wiener filter is the type of filter to use to produce an estimate of the desired or random process of the target by linear time-invariant (LTI) filtering of these observed noisy process, assuming the known stationary signal and noise spectra, and additive noise. The wiener filtering is optimum in the manner of the mean square error. In other words, what can be said that the wiener reduces the overall error in the process of the inverse filtering and smoothen noise.

HISTOGRAM EQUALIZATION

The histogram equalization is one method used to process images by modifying the intensity distribution of histogram in order to adjust the contrast of these images. The main objective of this technique is to give a linear trend to the cumulative probability functions associated to the processed images.

As simply as it can be explained, the processing of the histogram equalization depends on the uses of the cumulative probability function (CDF). The CDF is a cumulative sum of all the probabilities in the domain is explained by:

$$cdf_x(i) = \sum_{j=0}^{i} P_x(j) \qquad\qquad (7)$$

The main idea of this processing step is it to give to the resulting image in a linear cumulative distribution function.

IV. EXPERIMENT AND RESULTS

For The simulated dataset is constructed by using gprMax simulation tool which has the ability of simulating real commercial antennas. In all simulations, Geophysical Survey Systems Inc. (GSSI) 1.5 GHz (Model 5100) antenna is used. It can implement various scenarios with different objects, different soil types, and different burial depths. Therefore, a huge dataset including many GPR images is easy constructed. Here, gprMax was implemented and study a simple and general case, which is:

- Our box is $480 \times 148 \times 170 \; mm$, A sphere with a radius 10mm filled with water was placed at $240 \times 74 \times 100 \; mm$ in that box.

- With GSSI 1.5 GHz antenna placed on top of the box 5mm height scanning every 5mm, during simulation the antenna moved approximately 56 times, each time an A-Scan was collected to form the B-scan data.

- The Fresh Water coefficients are the ε_r: 80.0, σ :0.5, μ_r: 1.0, Magnetic loss: 0.0.

- Different soil situations were implemented, the first scenario is having the box filled with sand and placing the sphere in it. With Sand coefficients having these values for this experiment: ε_r: 3, σ :0.001, μ_r: 1.0, Magnetic loss: 0.0.

- • Second scenario some roughness has been added to the box (valleys are now up to 5mm deep and peaks are up to 5 mm tall), using soil Peplinski a soil and sand and clay fraction 0.5, bulk density $2g/[cm]^3$, sand practical density of 2.66 $g/[cm]^3$ and volumetric water fraction of 0.001-0.25 .

- • Third scenario 300 blades of grass have been added on top of the same box with various heights between 30 to 50 mm with same soil properties as the second scenario.

In the GPR system to work as effective as possible, it is best to visit the area in question prior to any mapping or profiling for obtaining not only geological information but also historical and present land use. The main objective of this research is to enhance the GPR collected data and reducing the clutter and noises from other unwanted signals. PSNR (Peak- Signal to Noise Ratio) has been used to evaluate the difference made by these listed algorithms

So, the first step to calculate our PSNR, first the mean square error will be collected, then sum these mean square errors and divide them by the number of matrix elements (rows* columns) [18].

$$MSE = \frac{1}{mn}\sum_{i=0}^{m-1}\sum_{j=0}^{n-1}\|I(i,j) - K(i,j)\|_2^2 \qquad (8)$$

Then PSNR is expressed by:

$$PSNR = 10 \times \log_{10}\left(\frac{MAX_I^2}{MSE}\right) \qquad (9)$$

In GPRmax simulation the geometrical structure of the cases has been under study is shown in Figure. 2. During this simulation A-scan has been collected to provide the B-scan images by moving the antenna approximately 56 times.
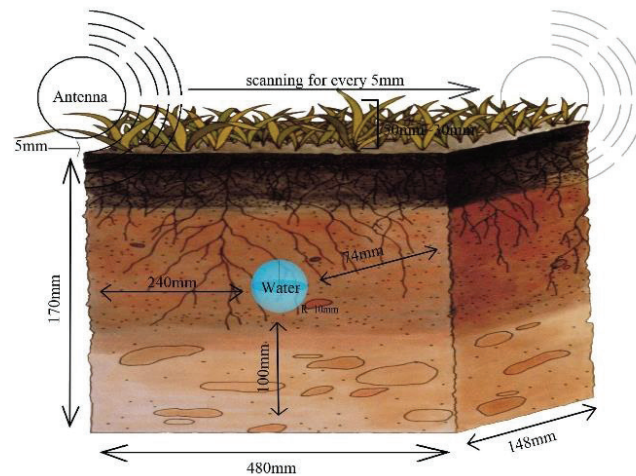
Figure 2: The geometric structure of the box.

The simulated B-scan soil and fresh water situation compared to the data collected from same box of soil without injecting water are shown in Figure. 3 below.
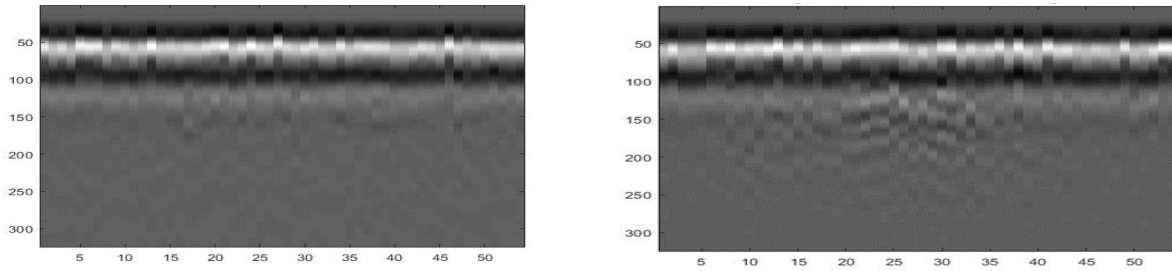
Figure 3: Shows the original image (B-Scan) of soil and soil with water sequentially.

The GPR Image data size is 325 with feature dimension 54, i.e., 325×54. And as known representation of the clutter component in GPR is stronger than the target. The simplest clutter removing method MS effect for soil and fresh water its corresponding power spectrum in Figure.4.

While Figure (5- 8) shows the decluttering results of SVD, PCA, ICA, and PICA and their power spectrum for the first data set of soil and fresh water scenario. While Figure 9 shows how the filters effect the GPR image.

Table1 summarize the PSNR Performance for all Decluttering algorithms and filters.

The experimental result for this scenario shows that the PICA algorithm performance exceeded the other subspace clutter remove methods. While with filtering Histogram showed a much better performance than the other applied filters.

(A)   (B)
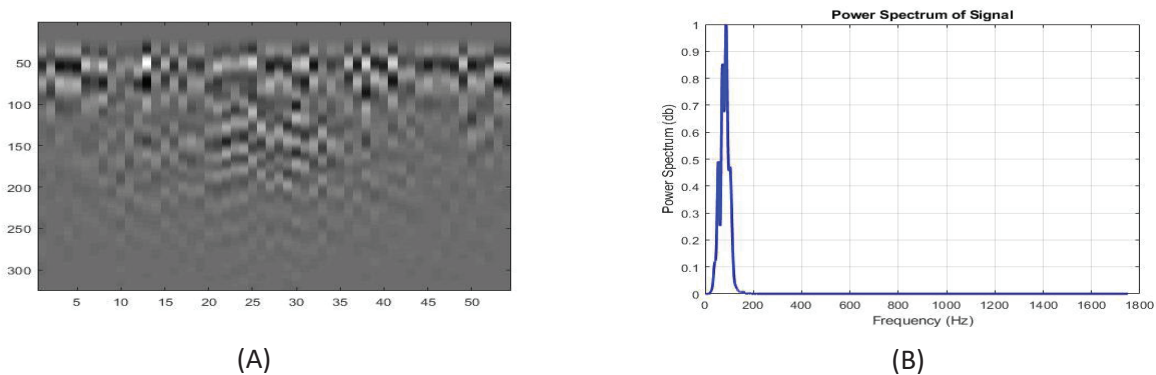
Figure 4: (A) Decluttering soil and fresh water image using MS (B) The power spectrum

(A)   (B)
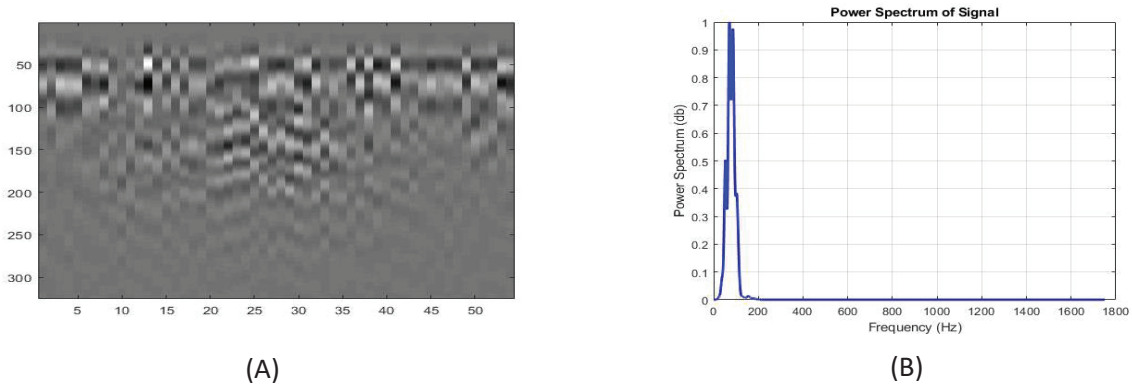
Figure 5: (A) Decluttering soil and fresh water image using SVD (B) The power spectrum.

(A)

(B)
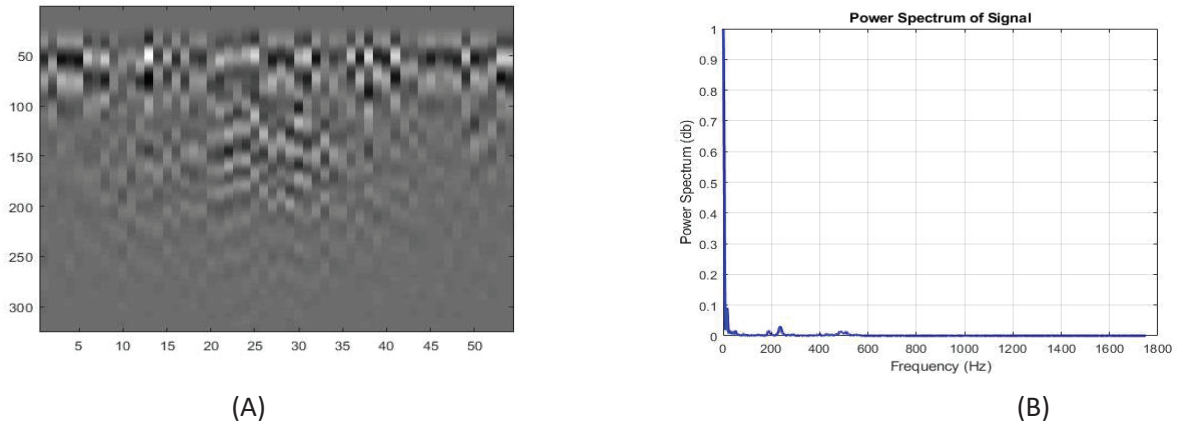
Figure 6: (A) Decluttering soil and fresh water image using PCA (B) The power spectrum.

(A)

(B)
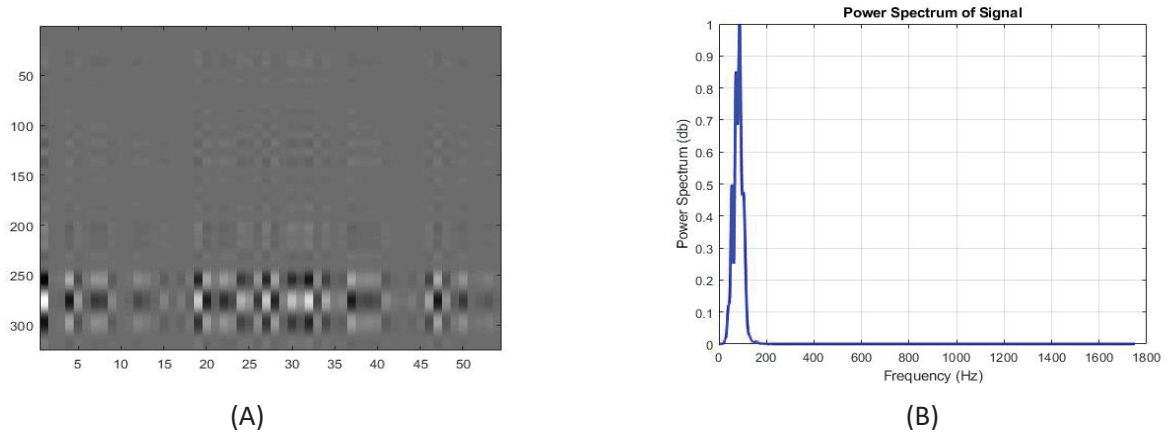
Figure 7: (A) Decluttering soil and fresh water image using ICA (B) The power spectrum.

(A)

(B)
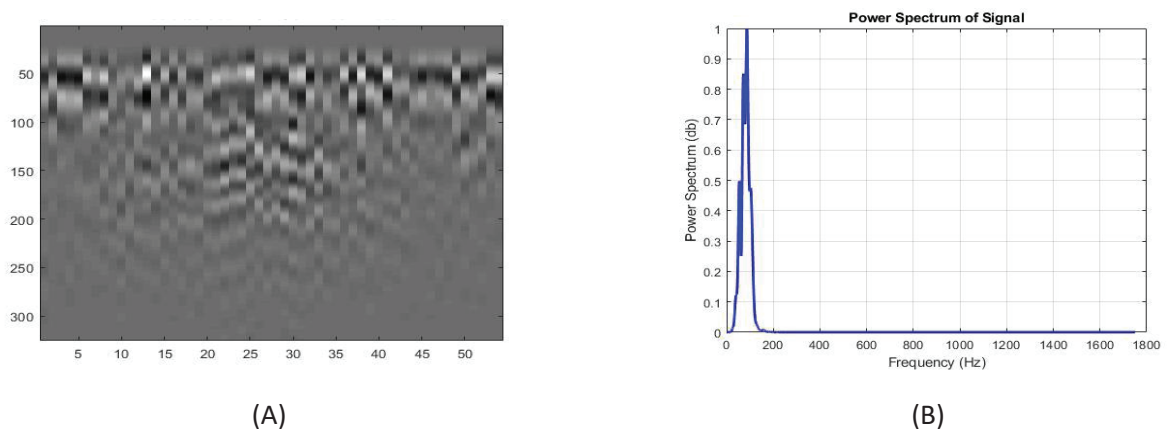
Figure 8: 7: (A) Decluttering soil and fresh water image using PICA (B) The power spectrum.
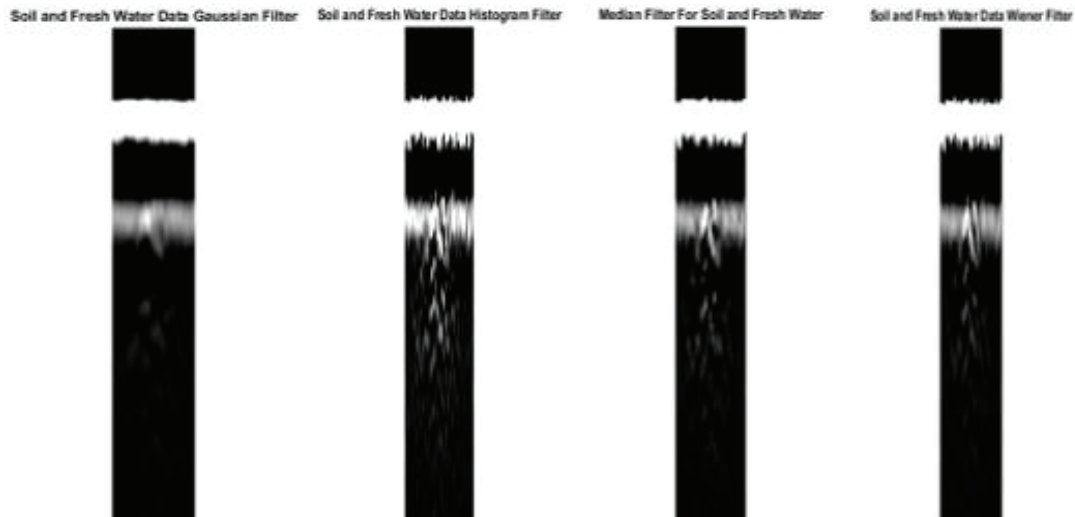
Figure 9: shows the effect of filtering over the soil and fresh water image.

TABLE 1: PSNR values for different described methods for soil and fresh water data

METHOD	PSNR	METHOD	PSNR
MS	57.1904	Gaussian	48.2118
SVD	64.4371	Median	48.0853
PCA	56.0816	Wiener	48.0106
ICA	64.7930	Histogram	52.9641
PICA	65.2304		

The simulated B-scan for soil roughness situation compared to the data collected from same box of soil without injecting water are shown in Figure. 10 below.

The simplest clutter removing method MS effect for soil and fresh water its corresponding power spectrum in Figure.11.

While Figure (12- 16) shows the decluttering results of SVD, PCA, ICA, and PICA and their power spectrum for the first data set of soil roughness and fresh water scenario. While Figure. 17 shows how the filters effect the GPR image. Table 2 summarize the PSNR Performance for all Decluttering algorithms and filters for the soil roughness data set. In the data set PCA and PICA with slit difference between them, their performance exceeded the other subspace clutter remove algorithms. While with filtering Histogram showed a much better performance than the other applied filters.
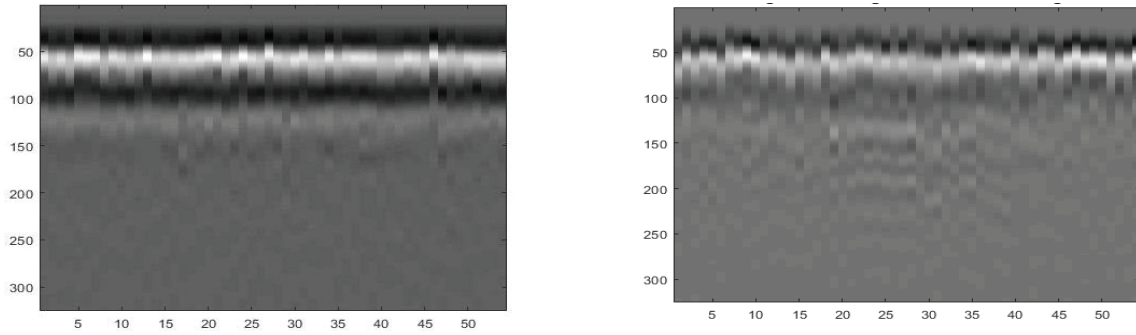
Figure 10: Shows the soil image and the soil and fresh water after adding some roughness.

As its obvious the after adding some roughness to our box the signal we received is a bit distorted which leads to have

unclear image because of new soil properties.

(A)

(B)
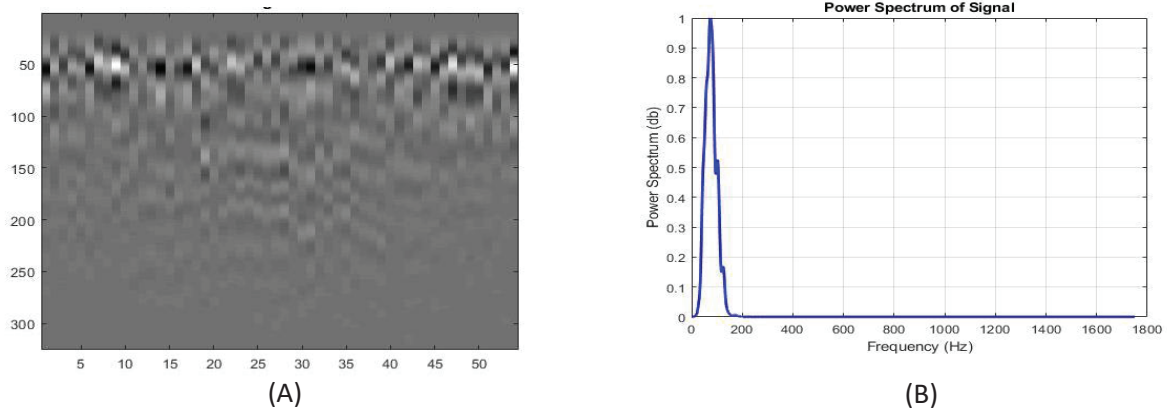
Figure 11: (A) Decluttered soil roughness image using MS (B) The Power spectrum.

(A)

(B)
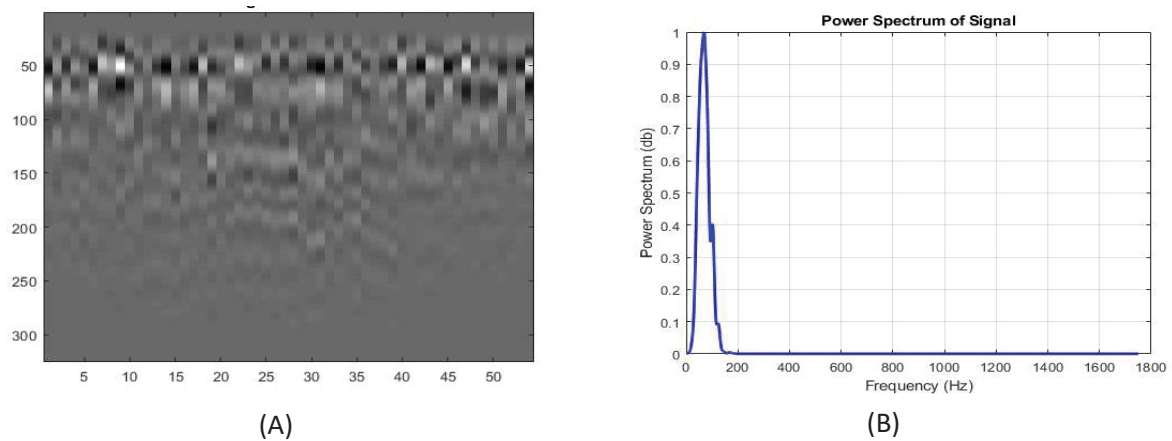
Figure 12: (A) Decluttered soil roughness image using SVD (B) The power spectrum.

(A)

(B)
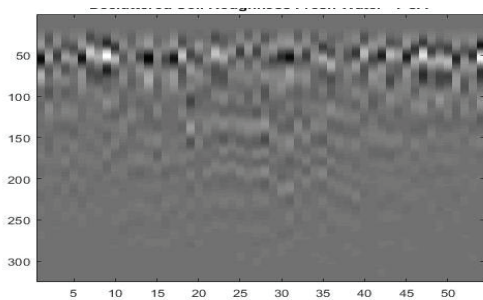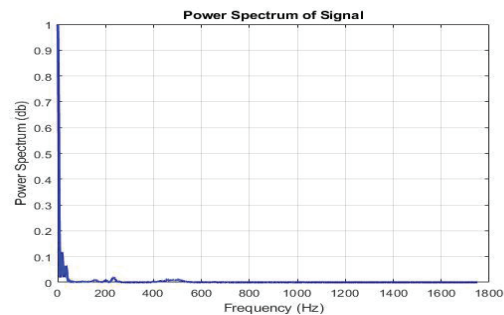
Figure 14: (A) Decluttered soil roughness image using PCA (B) The power spectrum.

(A)

(B)
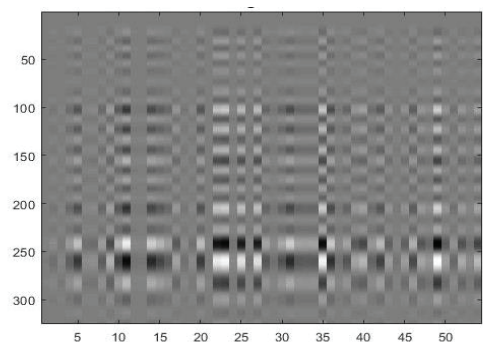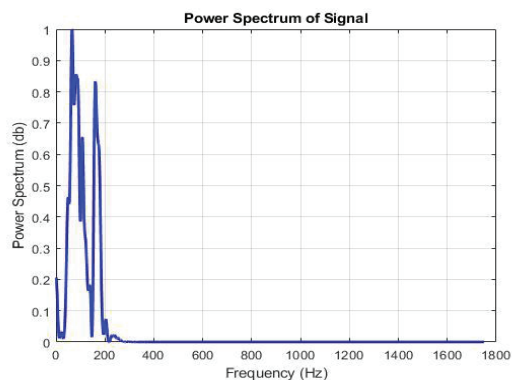
Figure 14: (A) Decluttered soil roughness image using ICA (B) The power spectrum.
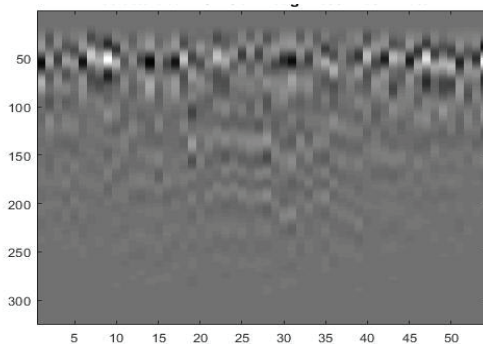
(A)
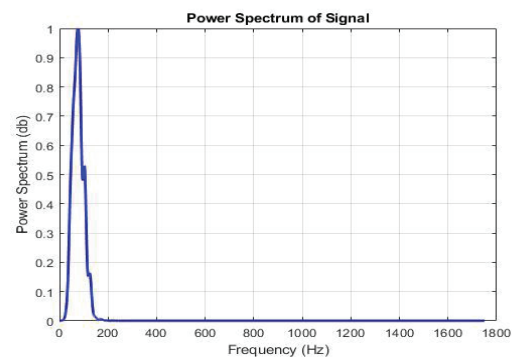
(B)

Figure 15: (A) Decluttered soil roughness image using PICA (B) The power spectrum.
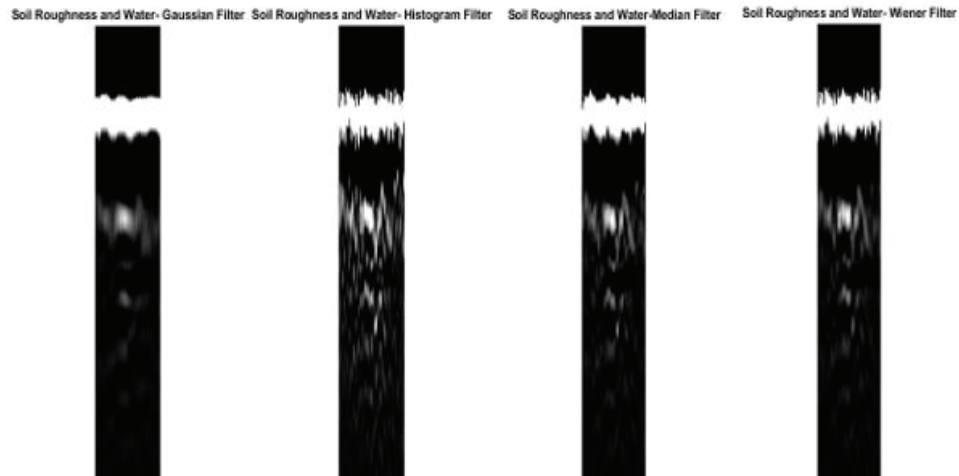
Figure 16: Shows the effect of the filters on the soil roughness image.

TABLE 2: PSNR values for different methods of the soil roughness data.

METHOD	PSNR	METHOD	PSNR
MS	58.9175	Gaussian	48.7414
SVD	69.3546	Median	48.4714
PCA	70.5059	Wiener	48.2815
ICA	66.6977	Histogram	53.4258
PICA	70.4988		

The simulated B-scan for grass soil situation compared to the data collected from same box of soil without injecting water are shown in Figure. 17 below.

The simplest clutter removing method MS effect for soil and fresh water its corresponding power spectrum in Figure.18.

While Figure (19- 22) shows the decluttering results of SVD, PCA, ICA, and PICA and their power spectrum for the first data set of soil roughness and fresh water scenario. While Figure. 23 shows how the filters effect the GPR image. Table 3 summarize the PSNR Performance for all Decluttering algorithms and filters for the soil roughness data set.

In this data set PICA algorithm performance exceeded the other subspace clutter remove algorithms. While with filtering Histogram showed a much better performance than the other applied filters
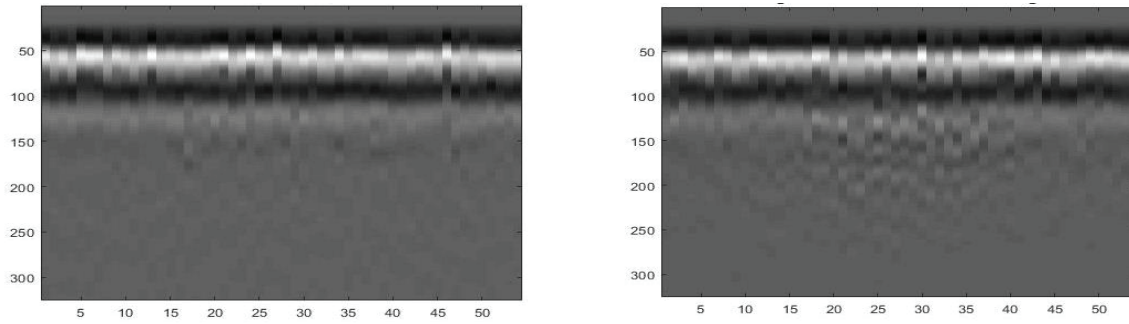
Figure 17: Shows the soil image and the soil and fresh water after adding grass on top.

(A)   (B)
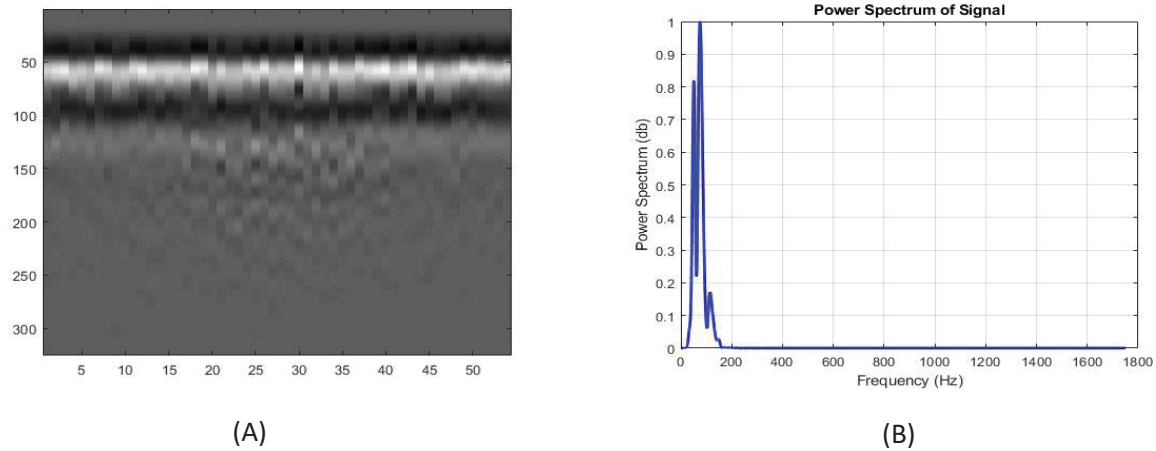
Figure 18: (A) Decluttered grass soil image using MS (B) The power spectrum.

(A)

(B)
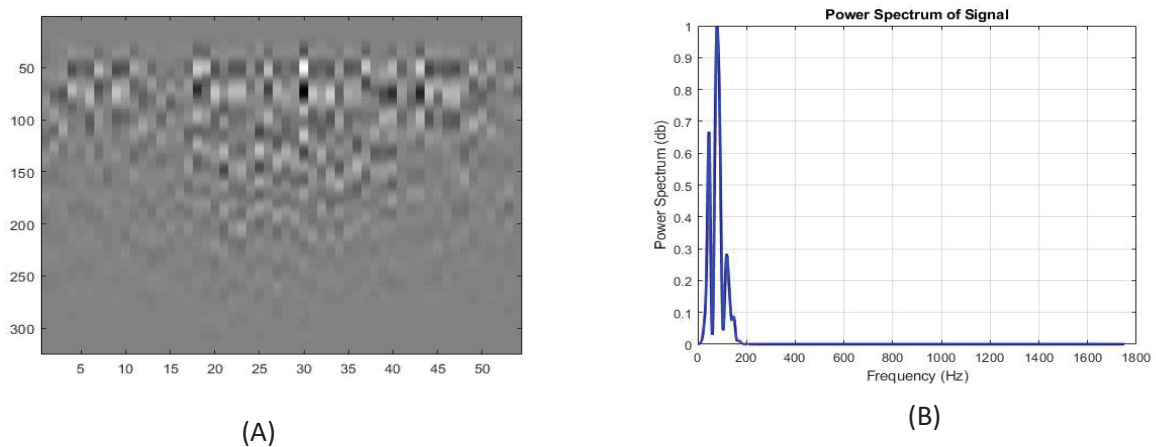
Figure 19: (A) Decluttered grass soil image using SVD (B) The power spectrum.
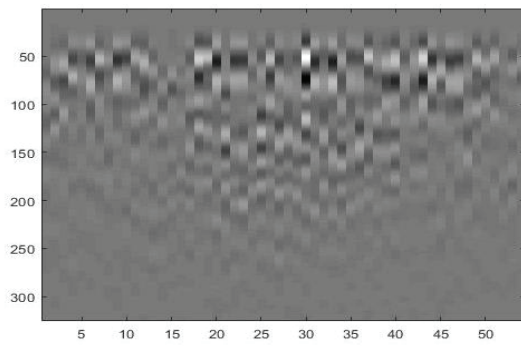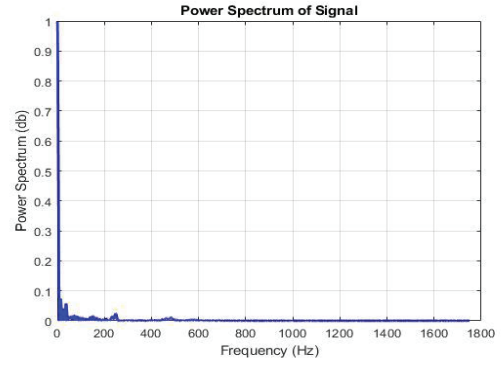
(A)   (B)

Figure 20: (A) Decluttered grass soil image using PCA (B) The power spectrum.
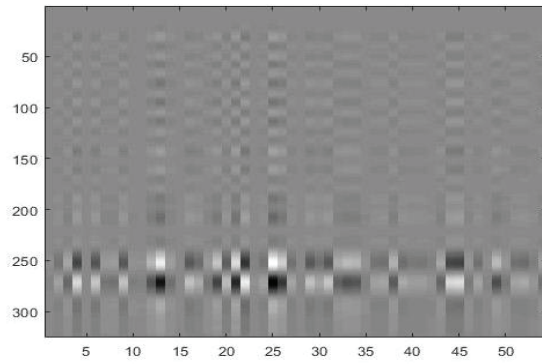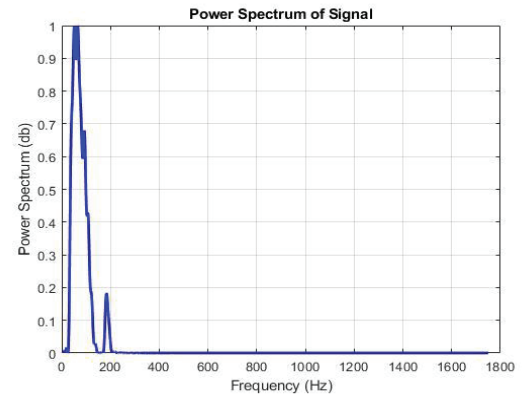
(A)   (B)

Figure 21: (A) Decluttered grass soil image using ICA (B) The power spectrum.
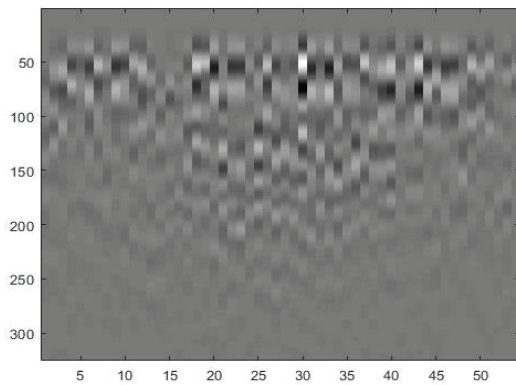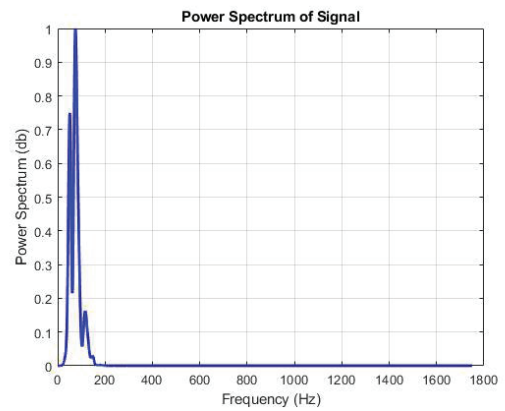
(A)   (B)

Figure 22: (A) Decluttered grass soil image using PICA (B) The power spectrum.
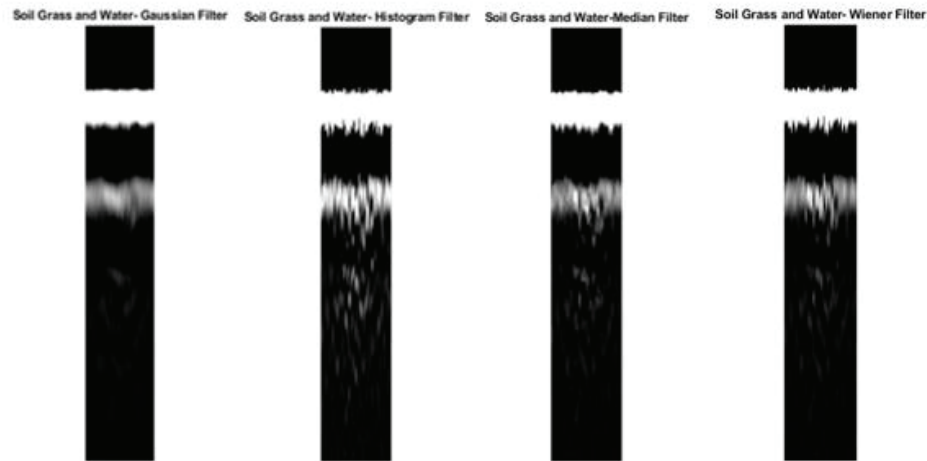
Figure 23: Shows the effect of filters on the Grass soil image.

TABLE 3: PSNR values for different methods on the grass soil data.

METHOD	PSNR	METHOD	PSNR
MS	57.3919	Gaussian	48.3540
SVD	62.7766	Median	48.2273
PCA	56.3077	Wiener	48.1700
ICA	61.4543	Histogram	53.0424
PICA	64.1537		

All subspace algorithms and filters are simulated using MATLAB (R2017b) software tool. For all the decomposition methods, the results are satisfactory and they can remove the background and surface clutter successfully. In addition, it can reduce the dimensionality of the processed data. Meanwhile filtering the GPR image alone can be sometimes not enough.

V. CONCLUION

The signal processing is required to analyze the collected signals, here different methods to analyze and find water with the best method used in different soil situation some methods like mean subtraction (MS), singular value decomposition (SVD), principal component analysis (PCA), independent component analysis (ICA), and the combination (PICA) were tested and examined for the GPR clutter reduction purpose and image enhancement filters such as Gaussian, Median, Wiener, Histogram. They have been applied to GPR data with the aim to improve image quality by removing target unwanted features from the image and presents reduced data for further processes like classification tasks which is known to be the next stage after clutter reduction. As demonstrated earlier these methods have shown satisfying results in the term of clutter and noise removing. In the first soil situation methods like SVD,

ICA and PICA have provided better results, while after adding some roughness SVD, PCA, and PICA, after adding the grass on top results showed that SVD and PICA were much better. We can conclude that PICA was our optimal algorithm regarding these soil situations. Meanwhile in filtering Histogram showed a much more satisfying result than the other filters.

REFERENCES

[1]   H.M.Jol, "Ground Penetrating Radar: theory and applications", Elsevier Science, Radarweg 29, PO Box 211, 1000 AE Amsterdam, The NetherlandsThe Boulevard, Langford Lane, Kidlington, Oxford OX5 1GB, UKFirst edition 2009:5-30

[2]   Daniels, D.J. (Ed.), "Ground Penetrating Radar (2nd Edition)", IEE, ISBN 0-86341-360-9, London, UK, 2004.

[3]   Erica Carrick Utsi, "Ground Penetrating Radar: Theory and Practice",Elsevier Science,2017: 1-33.

[4]   Jeff Ambrose Mitchell, "Introduction to Locating Buried Utilities", Mar 11, 2009.

[5]   Mohanad Abd Shehab, Mohammed Abdulridha Sahib Al Obaidi, Ilknur Hoş, and Saeid Karamzadeh, "Subspace Clutter Removal Techniques in GPR Images", Progress In Electromagnetics Research M, Vol 82, 2019

[6]   Cansu Eren, Saeid Karamzadeh, Mesut Kartal, "The artifacts of human physical motions on vital signs monitoring", 2019 Scientific Meeting on Electrical-Electronics & Biomedical Engineering and Computer Science (EBBT), April 2019, DOI: 10.1109/EBBT.2019.8741668.

[7]   Karamzadeh, Saeid, Mesut Kartal, Sedef Kent, and A. Abed Ashtiyani. "Optimal Signal Processing Method in UWB Radar for Hidden Human Detection." In EUSAR 2014; 10th European Conference on Synthetic Aperture Radar, pp. 1-3. VDE, 2014.

[8]   Karamzadeh, Saeid, and Mesut Kartal. "UWB radar in hidden human detection." International Journal of Electronics, Mechanical and Mechatronics Engineering (IJEMME) 3, no. 2 (2013): 579-583.

[9]   Saeid Karamzadeh , Cansu Büyükhan, Umut Eskiçırak, Tarık Akyol, "OPTIMAL SIGNAL PROCESSING METHODS IN GPR" Department of Communication Systems, Satellite Communication & Remote Sensing, Istanbul Technical University, Maslak, 34469, Istanbul TURKEY

[10]   Zhu, J., W. Xue, X. Rong, and Y. Yu, "A clutter suppression method based on improved principal

component selection rule for ground penetrating radar," Progress In Electromagnetics Research M,Vol. 53, 29–39, 2017.

[11]   Karlsen, B., H. B. Sorensen, J. Larsen, and K. B. Jakobsen, "Independent component analysis for clutter reduction in ground penetrating radar data, detection and remediation technologies for mines and minelike targets VII," International Society for Optics and Photonics, Vol. 4742,378–390, 2002.

[12]   PO, Botstein D ,"Singular value decomposition for genome-wide expression data processing and modeling." Proc Natl Acad Sci USA (2000), 97, 10101-6.

[13]   Christian F. Beckmann and Stephen M. Smith," Probabilistic Independent Component Analysis for Functional Magnetic Resonance Imaging", FMRIB Technical Report TR02CB1, Oxford, UK, 2004.

[14]   Cichocki, A. and S. Amari, "Adaptive Blind Signal and Image Processing: Learning Algorithms and Applications", John Wiley & Sons, West Sussex, UK, 2003.

[15]   Thirion, N., J. Mars, and J. L. Boelle, "Separation of seismic signals: A new concept based on a blind algorithm," Signal Processing VIII, Theories and Application, 85–88, Elsevier, Triest, Italy, September 1996.

[16]   Tinku A. , Ajoy K. Ray **, "**Image Processing principle and applications",2005:105-129.

[17]   James D. Broesch, "Digital Signal Processing", 2009 :125-134.

[18]   Bill Comstock, "Using PSNR thresholds to modulate the degree of lossy compression in JPEG2000 files", May 2011.

Comparison of Spi, Spei and Sri Drought Indices for Seyhan Basin

Mehmet DİKİCİ[1], Murat AKSEL[2]

Abstract - Today, mitigation of the adverse impacts of drought has gained considerable importance in the context of the management of water resources, which is adversely affected by climate change. In this context, to be able to achieve drought risk analyses, meteorological and hydrological data should be sufficient; if they are not, they should be completed. Seyhan Basin spread across the Seyhan River to an area of 2.203.544 ha, extending from Sivas to the Eastern Mediterranean. With 22.035 km^2, the basin area constitutes 2.07% of Turkey's surface area. In this study, by using the meteorological and hydrological data of Seyhan basin between 1970 and 2016, drought risk analyses of the basin with the most widely used around the world SPI, SRI and SPEI drought indices were discussed. In first step of this study, incomplete data was completed with regional analyses. According to these indices, drought severity and magnitude were found. Analyses were performed according to 1, 3, 6, 9, 12, 18, 24, 48-month repeat intervals. Classification of droughts and threshold values were determined. The indices were compared, the correlation between them was examined, and drought risk analyses and drought maps were made separately for each index.

Keywords: Basin, water resources, drought index, SPI, SRI, SPEI

[1] *Department of Civil Engineering, Alanya Alaaddin Keykubat University, Alanya, Antalya, Turkey, mehmet.dikici@alanya.edu.tr,* https://orcid.org/0000-0001-5955-3425
[2] *Department of Civil Engineering, Alanya Alaaddin Keykubat University,* *murat.aksel@alanya.edu.tr,* https://orcid.org/0000-0002-6456-4396

1. Introduction

Today, mitigation of the expected impacts of drought is vitally important in the context of the planning, development and management of the water resources, which is adversely affected by climate change. Management of increasing drought risk and adaptation to it can only be achieved through the development of sustainable and effective water management strategies that adopt holistic approaches [1]. Management of water resources is also important in terms of meeting the energy needs [2]. Drought risk management is an important part of water resources management policies and strategies. Drought management is also a part of the disaster management [3]. Drought risk management is the process of prevention and mitigation concept and effort against the negative consequences of drought hazard and the potential disaster effects through activities and measures for prevention, mitigation of damage and preparedness [4]. National drought policies play a major role in managing the drought risk [5]. Research on how the negative impact of climate change on the environment, especially on water resources will be shed light on the measures that should have been taken in the future [6]. In order to reduce the impacts caused by drought, drought management plans need to be prepared based on country legislation and by taking into account the specific drought characteristics and impacts of the basin [7, 8]. In order to create integrity, it is very important that these plans are prepared as part of the basin management plan. The objective here is to provide information at an early time before or during the onset of drought, within a drought risk management plan, in order to reduce potential impacts [9]. Because drought is a slow-starting and progressing hydrological phenomenon, monitoring and analysis of the drought are of great importance. In this study, the comparison of SPI, SPEI and SRI drought indices and their compatibility for Seyhan Basin were analyzed. For this purpose, meteorological, hydrological and hydrogeological data between 1970 and 2016 were based on.

2. Material and Method

Seyhan Basin spread across the Seyhan River to an area of 2.203.544 ha, extending from Sivas to the Eastern Mediterranean. With 22.035 km^2, the basin area constitutes 2.07% of Turkey's surface area.

Standardized Precipitation Index (SPI): SPI, which is the most common used meteorological drought index, is an index based on precipitation for different time periods and ignoring other effects [10].

While negative values show lack of precipitation, positive values show excess precipitation. The severity of drought can be classified according to the size of negative SPI values. SPI drought classes are obtained from the normally distributed precipitation series. By dividing the difference between the precipitation on a specific time scale and the average precipitation by the standard deviation of the series, SPI is calculated as equation 1.

$$SPI = \frac{x_i - x_j}{\sigma} \tag{1}$$

where x_i is existing precipitation in the examined period, x_j is the average precipitation of the series and σ is the standard deviation of the series. With SPI, it is possible to express the lack of precipitation in more than one time scale. The lack of precipitation in different time scales can be effective on different water sources. For example, while the moisture of the ground may be affected by lack of precipitation in a shorter period of time, the storage may be affected in a longer period of time. Therefore, SPI can be calculated on 3, 6, 9, 12, 18, 24 and 48-month time scales. SPI-3 can be used to understand short and medium term humidity conditions, SPI-6 can be used to understand medium term precipitation trends, SPI-9 can be used for medium term precipitation patterns and SPI-12 can be used to understand long term precipitation patterns [11, 12]. The fact that SPI can be calculated for different time intervals has allowed this index to be applied in different areas. Therefore, SPI can provide detection of different types of drought. Based on long-term precipitation observations, SPI is calculated for a specific location and the desired duration. The following steps were followed when calculating SPI;

1. Conversion of probability distribution function of raw precipitation data to gamma probability distribution function,

2. Calculation of standardized precipitation sequences (that is, SPI values) for the precipitation probability obtained from the gamma probability distribution function, by using the reverse-standard normal distribution function [13].

Drought severity is the absolute value of the sum of the SPI values of each month in which the drought event occurs. Table 1 shows the levels of drought and threshold values proposed and widely used in the literature [9] for SPI.

Table 1. Standard Precipitation Index (SPI) drought classification and threshold values

Threshold values	Drought severity
2 and above	Excessive humidity
1,5 — 1,99	Very humid
1 — 1,49	Moderate humidity
-0,99 — 0,99	**Normal**
-1 — -1,49	Moderate dry
-1,5 — -1,99	Severe dry
< -2	Excessive dry

Standardized Precipitation Evapotranspiration Index (SPEI): Comparing the other indices, the Standardized Precipitation Evapotranspiration Index (SPEI) is a newer drought index. SPI is based on two main assumptions;

1- The importance of precipitation is much higher than other variables that may affect the severity of drought.

2- Drought is controlled only by the temporal variability emerging in precipitation.

In the calculation of SPEI, although it is based on the principles of SPI, the effect of temperature on drought is also taken into consideration as different from SPI and superior to it. Therefore, SPEI is an ideal index in the examination of climate change with climate model projections.

SPEI is an index based on the values of precipitation, potential transpiration and evaporation. Thus, SPEI can take into account the changes in evaporation values depending on the temperature change. SPEI calculation requires both precipitation data and complete time series data for potential evapotranspiration. Because of this, it is not possible to calculate SPEI where there is insufficient data. The longer the data, the stronger the calculation results [8]. SPEI considers the cumulative climatic water budget anomalies (precipitation - potential transpiration and evaporation). The SPEI calculation also covers the determination of the appropriate probability distribution of long-term observations (such as SPI) and the conversion of them to normal

distribution [14]. In this study, the method [15] was used to calculate the required potential transpiration and evaporation values in SPEI calculations because this method requires only monthly average temperature data. In the second phase, in the context of the equation given below; the potential transpiration and evaporation value (PET_i) calculated by using the method is subtracted from the precipitation value (P_i) for the investigated month, and then, a simple criterion (D_i) is obtained for the excess water or shortage of it in that month:

$$D_i = P_i - PET_i \tag{2}$$

In the third phase, the values of D_i are converted to the log-logistic probability distribution function. In the fourth and final phase, D_i series (that is SPEI values), which has been standardized, as in SPI, by using the inverse-standard normal distribution function for the probabilities of access or shortage of water (D_i) obtained from the log-logistic probability distribution function, is obtained. SPEI can be calculated monthly for time intervals ranging from 1 month to 48 months or more. For the SPEI, the drought severities and threshold values commonly used in the literature are given in Table 2.

Table 2. Standardized Precipitation Evapotranspiration Index (SPEI) Drought classification and threshold values

Threshold values	Drought severity
2 and above	Excessive humidity
1,5 — 1,99	Very humid
1 — 1,49	Moderate humidity
0,5 – 0,99	Close to normal humidity
-0,499 — 0,499	**Normal**
-0,5 — -0,99	Close to normal dry
-1 — -1,49	Moderate dry
-1,5 — -1,99	Severe dry
< -2	Excessive dry

Standardized Runoff Index (SRI): SRI is a drought index developed in 2008 as an expression of hydrological drought and based on SPI methodology. As distinct from SPI, runoff data (river discharge data) is used in SRI calculation. Dividing the difference between the runoff values for a specific time scale and the average runoff value by standard deviation of the series, SRI is calculated as equation 3.

$$SRI = \frac{x_i - x_j}{\sigma} \tag{3}$$

where x_i is existing runoff in the examined period, x_j is the average runoff of the series and σ is the standard deviation of the series. Sri is an index that is easy to calculate as SPI because it only requires the use of runoff data. SRI, such as SPI, can be calculated daily or monthly by using both observed and predicted runoff data. Thus, information about high and low runoff periods related to flood and drought can be obtained. Thanks to SRI, hydrological conditions can be monitored in multiple time scales for a place [8]. SRI results can be evaluated in comparison with SPI analysis of the same region. A strong relationship between SPI and SRI was observed in the studies conducted to see the relationship between precipitation and runoff [16]. When calculating the SRI, it is important that the stations represent the basin and that the runoff series are natural. While examining the hydrological drought in drought analyses, 9-12-month SRI results are preferred because they reflect a complete hydrological precipitation period. Table 3 shows drought severity and threshold values used commonly in the literature for SRI. Because the calculation method of SRI was same with the calculation method of SPI and SPEI, similar threshold values were used.

Table 3. Standardized Runoff Index (SRI) drought classification and threshold values

Threshold values	Drought severity
2 and above	Excessive humidity
1,5 — 1,99	Very humid
1 — 1,49	Moderate humidity
-1 — 1	**Normal**
-1 — -1,49	Moderate dry
-1,5 — -1,99	Severe dry
< -2	Excessive dry

Drought Classification and Threshold Values Used for Drought Analysis of Seyhan Basin: In the scope of Seyhan Basin drought analysis studies, four main drought severity classes were used to allow consistent comparison of all indices instead of the drought severity and threshold values preferred in the literature to use for the indices whose methods were described in this section: These were determined as severe drought, moderate severe drought, mild drought, no drought-normal/humid. Table 4 shows the drought classification and threshold values of the indices used in the context of the drought analysis study in Seyhan Basin.

Table 4. Drought classification and threshold values used for drought analysis of Seyhan Basin

SPI, SPEI, SRI	Drought Classes
> -0,99	(no drought-normal/humid)
-1,49 — -1	(mild drought)
-1,99 — -	(moderate severe drought)
< -2	(severe drought)

1, 3, 6, 9, 12, 18, 24 and 48-month values belonging to Standardized Precipitation Index (SPI) were calculated for stations in the basin. Then, weighted averages of these values were obtained to cover the entire Seyhan Basin, and they were regionalized. SPI drought severity time series of Seyhan Basin is shown on Figure 1. In the series, the blue periods represent normal and above (humid) periods and red periods represent dry periods.
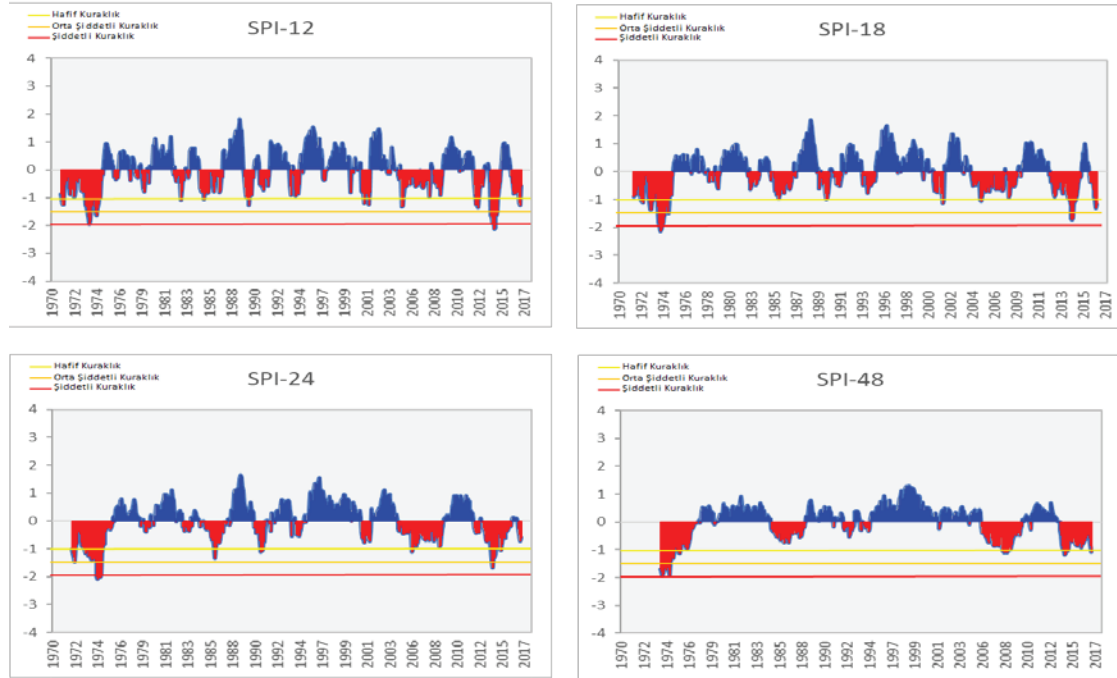
Figure 1. Seyhan Basin SPI drought severity time series

The Standardized Precipitation Evapotranspiration Index (SPEI) and Standardized Runoff Index (SRI) were calculated in different periods (1, 3, 6, 9, 12, 18, 24 and 48-month), and the time series of the SPEI values calculated for the basin were found. Values for the basin were obtained by taking weighted averages of SPEI and SRI values, which were calculated based on stations in the basin, to cover the entire Seyhan Basin and they were regionalized.

3. Results and Discussion

The aim of this study was to present drought risk analysis created by using calculated meteorological and hydrological indices. The meteorological, hydrological and agricultural drought was analyzed by the values of the Standardized Precipitation Index (SPI – 1, 3, 6, 9, 12, 18, 24 and 48-month), the Standardized Precipitation Evapotranspiration Index (SPEI – 1, 3, 6, 9, 12, 18, 24 and 48-month) and the Standardized Runoff Index (SRI – 1, 3, 6, 9, 12, 18, 24 and 48-month). Risk analysis of 12-month index values was carried out in order to represent the past drought periods consistently. In Seyhan Basin, the calculated drought indices for the determination

of the dry periods of the past were examined in detail and with this study it was aimed to determine the common periods between the indices . The method used is described below:

1- 24 drought indices selected for the comparison for the purpose of determining the dry periods were listed monthly by bringing them to the same time period for the time frame (1970 – 2016) examined within the scope of this report.

2- It was calculated whether the basin-wide was dry above normal by taking the area weighted average of each index for the basin and using its own parametric drought classification. At this level, it was only determined whether drought occurred or not; the severity of drought itself was not investigated. The color scale used in the charts is based on the common classification determined for drought indices; white color is normal and above (humid), yellow color is mild drought, orange color is moderate severe drought, red color is severe drought indicator.

3- It was aimed to determine the period of common drought in the chart by comparison between indices and examine within the scope of this study. In this context, dry periods in various lengths in 1973-1974, 1989, 2001, 2007-2008, 2014 and 2016 were determined for Seyhan Basin.

In the scope of the study, agricultural, hydrological and meteorological drought analyses were carried out with the help of indices by using the data available for 47 years of time period between 1970 and 2016. This study was carried by using a total of 24 indices: The Standardized Precipitation Index (SPI1, SPI3, SPI6, SPI9, SPI12, SPI18, SPI24, SPI48), the Standardized Precipitation Evapotranspiration Index (SPEI1, SPEI3, SPEI6, SPEI9, SPEI12, SPEI18, SPEI24, SPEI48) and the Standardized Runoff Index (SRI1, SRI3, SRI6, SRI9, SRI12, SRI18, SRI24, SRI48). The threshold values corresponding to the normal and above condition, mild drought, moderate-severe drought and severe drought classes of each index were determined and all analyses were performed taking into account these values. For all indices, risk analysis was performed by determining the percentages of incidence corresponding to drought classes. Risk analysis was conducted for both stations and the basin.

Results were determined by maps and graphs. It was observed that the indices calculated within the scope of the study had high relations with each other. It was determined that the indices calculated for the same periods shows a higher correlation than those calculated for the different periods. The comparison of the indices with each other is presented in Figure 2.
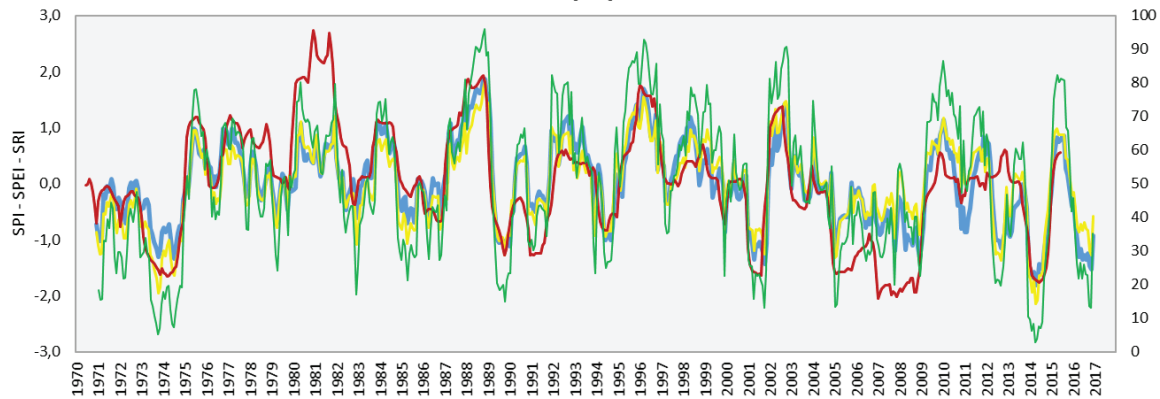
Figure 2. The comparison of SPEI12, SPI12 and SRI12 of Seyhan Basin (12-month)

4. CONCLUSION

As a result of the examination of all indices together, the periods in which the indices indicated the drought for Seyhan Basin in common were determined as 1973-1974, 1989, 2001, 2007-2008, 2014 and 2016. It was observed that the indices based on precipitation, runoff and evaporation values are compatible with each other. It was also proved in Seyhan Basin case that the indices in the same period gave very close results. At the end of the study, it is seen that all indices used are compatible with each other and calculate approximately the same values, but the most compatible index with meteorological data is SRI index for this region.

Acknowledgements

References

[1] Yuksel, I. (2018). The South-Eastern Anatolia project factor on water management and energy demand in Turkey. Fresenius Environmental Bulletin. 27(1), 246-253.

[2] Gulbaz, S., et al. (2017). A calibrated hydrological model for Alibeyköy watershed in İstanbul, Turkey incorporating lid implementation. FEB-Fresenius Environmental Bulletin, 6112.

[3] Wilhite, D. (2000), *Drought: A global assessment Hazards and disasters: A series of definitive major works*. Routledge, New York.

[4] UNDP (2016). Drought Risk Management.

[5] Wilhite, D.A., Sivakumar, M.V., and Pulwarty, R. (2014). Managing drought risk in a changing climate: The role of national drought policy. Weather and Climate Extremes. 3, 4-13.

[6] Al-Safi, H.I.J. and Sarukkalige, P.R. (2017). Assessment of future climate change impacts on hydrological behavior of Richmond River Catchment. Water Science and Engineering. 10(3), 197-208.

[7] EC (2007), *Drought management plan report: including agricultural, drought indicators and climate change aspects European Commission Directorate of Environment*.

[8] Svoboda, M. and Fuchs, B. (2016). Handbook of Drought Indicators and Indices.

[9] McKee, T.B., Doesken, N.J., and Kleist, J. (1993). *The relationship of drought frequency and duration to time scales*. in *Proceedings of the 8th Conference on Applied Climatology*. American Meteorological Society Boston, MA.

[10] WMO (2012). Statement on the Status of the Global Climate in 2012. Geneva, Switzerland: World Meteorological Organization.

[11] Zargar, A., et al. (2011). A review of drought indices. Environmental Reviews. 19(NA), 333-349.

[12] Lloyd-Hughes, B. and Saunders, M.A. (2002). A drought climatology for Europe. International journal of climatology. 22(13), 1571-1592.

[13] Vicente-Serrano, S.M., Beguería, S., and López-Moreno, J.I. (2010). A multiscalar drought index sensitive to global warming: the standardized precipitation evapotranspiration index. Journal of climate. 23(7), 1696-1718.

[14] Van Loon, A.F. (2015). Hydrological drought explained. Wiley Interdisciplinary Reviews: Water. 2(4), 359-392.

[15] Thornthwaite, C.W. (1948). An approach toward a rational classification of climate. Geographical review. 38(1), 55-94.

[16] Sheffield, J. and Wood, E.F. (2008). Projected changes in drought occurrence under future global warming from multi-model, multi-scenario, IPCC AR4 simulations. Climate dynamics. 31(1), 79-105.

INTERNATIONAL JOURNAL OF ELECTRONICS, MECHANICAL AND MECHATRONICS ENGINEERING

Submission Instructions

The scope of International Journal of Electronics, Mechanical and Mechatronics Engineering (IJEMME) covers the novel scientific papers about Electronics, Image Processing, Information Theory, Electrical Systems, Power Electronics, Control Theory, Embedded Systems, Robotics, Motion Control, Stochastic Modeling, System Design, Multidisciplinary Engineering, Computer Engineering, Optical Engineering, Design Optimization, Material Science, Metamaterials, Heat and Mass Transfer, Kinematics, Dynamics, Thermo-Dynamics, Energy and Applications, Renewable Energy, Environmental Impacts, Structural Analysis, Fluid Dynamics and related topics of the above subjects.

IJEMME is an international journal published four times a year (January, April, July and October). Manuscripts reporting on original theoretical and/or experimental work and tutorial expositions of permanent reference value are welcome. IJEMME Editorial Board is authorized to accept/reject the manuscripts based on the evaluation of international experts. The papers should be written in English.

The manuscript should be sent in electronic submission via IJEMME paper submission system of web address (www.aydin.edu.tr/ijemme)

Submission instructions of manuscripts.

Page Design: Text body area is (195mm x 275mm). 30 mm margin from top, 20 mm from down and 25 mm margin should be left on right/left sides.

Title should be in 16 pt. bold, capital letters with Times New Roman font in Microsoft Word format. Authors' names, affiliations, e-mail addresses should follow the title after double line spacing with authors' names and surnames in lower case except first letters in 14 pt, the rest is 10 pt. italic.

Abstract should not exceed 200 words with the word "Abstract" in 10 pt. italic, bold, abstract text in 9 pt. italic, all in Times New Roman font in Microsoft Word format.

Key Words not exceeding 5 should be in bold.

Document Character: Subtitles should be in 10 pt. bold, capital letters and text body 10 pt. both with Times New Roman font in Microsoft Word format. The manuscripts should be written on a single column, be double spaced with single line spacing between paragraphs. The subtitle of the first section should start after a single space following the keywords, the other subtitles also with a single line space following the text, there should also be single line spacing between the previous text and the subtitle.

Conclusion: section should have a title written in 1o pt. bold, capital letters and the text in 10 pt. all in Times New Roman font in Microsoft Word format.

Reference numbers should be given in brackets as illustrated below:

Referencing books:
[1]   Özsu M., T, Valduriez, P., *Principles of Distributed Database Systems*, Prentice Hall, New Jersey, 128-136,1991.

Referencing papers:
[2]   G. Altay, O. N., Ucan, "Heuristic Construction of High-Rate Linear Block Codes," *International Journal of Electronics and Communications (AEU),* vol. 60, pp.663-666, 2006.

Page number is to be placed at the top left corner of each page with pencil.
Length of the Manuscript should not exceed 20 pages excluding Figures and Tables.

INSTRUCTIONS ABOUT THE ACCEPTED MANUSCRIPTS:

Page Design: Text body area is (195mm x 275mm). 30 mm margin from top, 20 mm from down and 25 mm margins should be left on right/left sides.

Title should be in 16 pt. bold, capital letters with Times New Roman font in Microsoft Word format. Authors' names, affiliations, e-mail addresses should follow the title after double line spacing with authors' names in lower case and surnames in capital letter in 14 pt. the rest in 10 pt. in the same format.

Abstract should not exceed 200 words with the word "Abstract" in 12 pt. italic, bold, abstract text in 9 pt. italic, all in Times New Roman font in Microsoft Word format.

Key Words not exceeding 5 should be in 9 pt. bold.

Document Character: Subtitles should be in 10 pt. bold, capital letters and text body 10 pt. both with Times New Roman font in Microsoft Word format. The manuscripts should be written on two columns, be single spaced with single line spacing between paragraphs. The subtitle of the first section should start after a single space following the keywords, the other subtitles also with a single line space following the text, there should also be single line spacing between the previous text and the subtitle.

Sections: Formulas should be numbered sequentially. Referring to formulas should be as Eqn (.). Figures and Tables should be placed into the text body and captions for both should be 10 pt. Table numbers and captions should be placed before the Table. If necessary, both columns may be used for large Figures and Tables.

Conclusion section should have a title written in 12 pt. bold, capital letters and the text in 10 pt. all in Times New Roman font in Microsoft Word format. Conclusion should not be a version of the Abstract.

Reference numbers should be given in brackets as illustrated below:

Referencing books:
[1]   Özsu M., T, Valduriez, P., *Principles of Distributed Database Systems*, Prentice Hall, New Jersey, 128-136,1991.

Referencing papers:

[2]   G. Altay, O. N., Ucan, "Heuristic Construction of High-Rate Linear Block Codes*," International Journal of Electronics and Communications (AEU),* vol. 60, pp.663-666, 2006.

Short Biography of the authors should follow references after a single line space, names in 9 pt. surnames in 9 pt. and the text in 9 pt. The text should not exceed 100 words.